第 38 卷 第 2 期 新 型 炭 材 料 （中英文） Vol. 38 No. 2
2023 年 4 月 NEW CARBON MATERIALS Apr. 2023
Cite this : New Carbon Materials, 2023, 38(2): 283-304 **DOI:** 10.1016/S1872-5805(23)60722-X

Photothermal catalysis in CO_2 reduction reaction: Principles, materials and applications

ZHAO Shan-hai[1,†], WANG Hai-bing[1,†], LI Qiang[2], DING Hao[1], QIAN Cheng[1], WANG Qi[2], LI Hui-yu[1], JIANG Feng[1], CAO Hai-jing[1,*], LI Chun-he[2,*], ZHU Yan-yan[1,*]

(1. *College of Mathematics and Physics*, *Shanghai University of Electric Power*, *Shanghai* 200090, *China*;
2. *Department of Physics*, *Shaoxing University*, *Shaoxing* 312000, *China*)

Abstract: Reducing CO_2 emission has become one of the most urgent issues in the world. The use of abundant solar energy to convert carbon dioxide into carbon-based chemicals would be a tremendous advance. There are many papers on photocatalysis or thermal catalysis in the reduction of CO_2, however, there is little research on photothermal catalysis for this purpose. We summarize our current knowledge of this topic, and the classification of catalysts (new carbon materials, oxide materials, metal sulfide materials, MOF materials, layered double hydroxide materials), their modification and their use in the reduction of CO_2 is discussed. Trends in the development of new catalysts are considered.

Key words: Photothermal catalysis; CO_2 reduction reaction; New carbon materials; MOF materials; Heterojunction

1 Introduction

At present, massive emissions of CO_2 caused by the overconsumption of carbon-based chemicals resulting in the environmental contamination have become more and more serious. Especially the problems such as global warming, melting of polar glaciers, and rising sea levels. Therefore, the exploitation of renewable energy and developing environmental protection methods for the effective reduction of atmospheric carbon dioxide has become one of the focuses of public concerns nowadays. Strenuous attempts have been made to convert carbon dioxide into valuable carbon-based chemicals, such as CO, CH_4, CH_3OH, C_{2+}, etc, to alleviate the energy crisis and diminish the green-house effect[1]. Various methods are developed for CO_2 conversions[2], such as thermal catalytic reaction, electrocatalytic reaction, and photocatalytic reaction. The electrocatalytic reaction has a high potential barrier and slow reaction kinetics[3]. Photocatalysis has limited utilization of solar energy, resulting in a low conversion rate of CO_2[4]. Thermal catalytic technology also has many problems such as high energy costs, strict requirements for reaction equipments, and difficulty in achieveling high product selection[5]. In recent years, scholars have attempted to introduce both light and heat into the reaction of CO_2 reduction. It's found that the coupling of solar and heat energy can effectively regulate the activity and selectivity of CO_2 reduction[6], which opens a new pathway for the full utilization of solar energy. Photothermal catalysis in the reduction of CO_2 involve the photothermal catalytic tool (reactors), the concept and principle, catalysts (materials, optimization), and the applications.

2 Photothermal catalytic reaction

The photothermal catalytic reaction is a promising strategy to reduce CO_2 emissions. Introducing heat in photocatalysis could reduce the thermal catalytic reaction barrier and then accelerate the diffusion of molecules, triger and promote electron-hole separation to improve the utilization of solar energy, and ultimately realize the higher efficient conversion of CO_2

Received date: 2022-09-28; **Revised date:** 2023-02-02

Corresponding author: CAO Hai-jing, Associate Professor. E-mail: caohj@shiep.edu.cn;
LI Chun-he, Associate Professor. E-mail: chunhe@whu.edu.cn;
ZHU Yan-yan, Professor. E-mail: yyzhu@shiep.edu.cn

Author introduction: †ZHAO Shan-hai and WANG Hai-bing contributed equally to this work.

at relatively mild conditions.

2.1 Photothermal catalytic reactors

A photothermal catalytic reactor is a place where chemical reactions take place and its parameters (such as size, luminousness, air impermeability, pressure, and flow rate) could affect the catalytic reaction rate and yield of products. Scholars have carried out a lot of research work on photothermal catalytic reactors. In 2010, Chueh et al. first applied CeO_2 with mesh porous ceramic foam to a solar thermal chemical reactor and photothermally catalyzes CO_2 and H_2O to CO and H_2 (Fig. 1(a))[7]. Ghuman et al. reported a gas-phase packed-bed flow reactor (Fig. 1(b))[8]. As we could see in Fig. 1, the fixed-bed experimental system mainly consisted of a gas supply part, a fixed-bed reactor, and a tail gas analysis part. In the test of CO_2 adsorption performance, the gas was passed into the CO_2 analyzer at the end of the fixed bed. Based on the CO_2 adsorption data recorded by the CO_2 analyzer, the CO_2 adsorption capacity can be calculated according to the formula (1)[9].

$$q = \frac{Q \times \rho}{M \times m} \times \int_0^t \left(\frac{c_{in} - c_{out}}{1 - c_{out}} \right) dt \times \frac{T_0}{T} \quad (1)$$

where, q is CO_2 adsorption capacity, mmol·g^{-1}. Q is the decarbonization reaction flow rate, mL·min^{-1}. ρ is CO_2 density, kg·m^{-3}. m is the mass of the catalyst, kg. M is the molecular weight of CO_2. c_{in} and c_{out} are respectively CO_2 volume fractions at the entrance and exit of the test system, %. T_0 is 273 K. T is the test temperature, K. t is time, min. After condensation, the reaction gas was passed into the gas chromatography analyzer (GC) at the end of the fixed bed. Based on the product concentration recorded by the gas chromatography[10], the CO_2 conversion and CH_4 selectivity of the catalyst were calculated according to Equations (2) and (3).

$$X_{CO_2} = \frac{n(CO_2)_{in} - n(CO_2)_{out}}{n(CO_2)_{in}} \times 100\% \quad (2)$$

$$S_{CH_4} = \frac{n(CH_4)_{out}}{n(CO_2)_{in} - n(CO_2)_{out}} \times 100\% \quad (3)$$

where X_{CO_2} is the CO_2 conversion rate, while S_{CH_4} is CH_4 selectivity, and n (x) in and n (x) out are components at the inlet and outlet of the test system, mL min^{-1}.

2.2 Classification of photothermal catalysis

The research of photothermal catalysis is mainly targeted toward energy, the environment, and other fields. Thermodynamic analysis shows that some complex photothermal catalysis reactions have high Gibbs free energy and can only be excited by UV light[11], which leads to limitations in the utilization of the full solar spectrum. There are two main considerations to maximize the use of the full solar spectrum. One is developing a kind of new catalysis that can absorb solar energy with an expanded absorption edge[12]. Another is finding a material with small Gibbs free energy in a catalysis reaction. How to make full use of solar energy, especially in the infrared region[13], is urgent because visible light accounts for less than 40% of the full spectrum of the

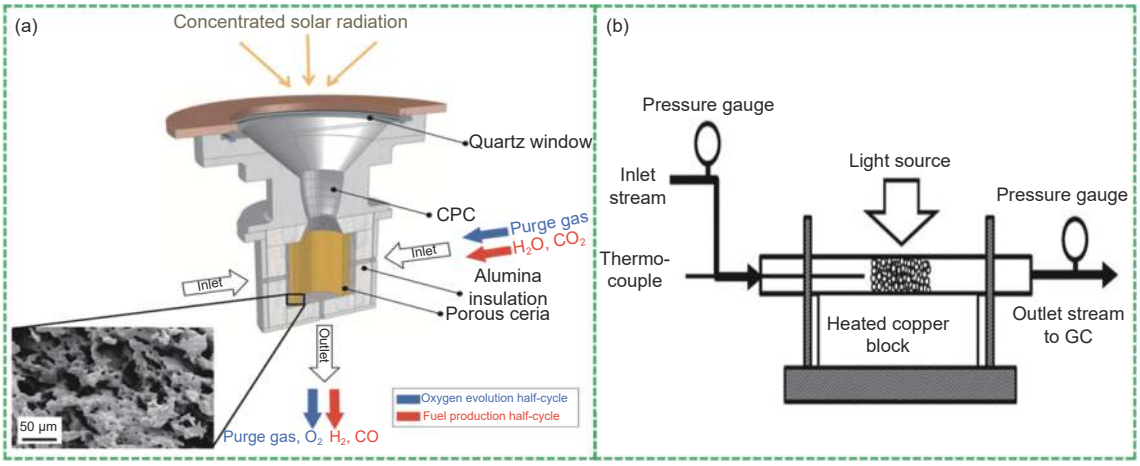

Fig. 1 (a) Schematic of the solar reactor for the two-step, solar-driven thermochemical production of fuels. Copyright 2010 by the American Association for the Advancement of Science. (b) Schematic diagram of the packed bed photoreactor. Copyright Royal Society of Chemistry 2015

sun and most of the left belongs to the infrared region. Many photothermal catalysts have been proposed correspondingly. Based on thermal-chemical or photochemical, photothermal catalysis reactions can be divided into three major mechanisms[14]: (i) thermal-assisted photocatalytic reaction; (ii) photo-assisted thermal catalytic reaction; (iii) photothermal co-catalysis. (Fig. 2(a)). The thermal-assisted photocatalytic reaction is mainly driven by optical energy, where the activation energy of photocatalysis is apparently reduced by thermal energy and then the mobility of the photocarrier or the mass transfer rate of reactants are promoted (Fig. 2(b)). For heat-assisted photocatalytic reactions, an external heating device and a transparent window should be designed for the photothermal reactor. The photothermal reactor can introduce light and heat in a controllable way. The photo-assisted thermal catalytic reaction (Fig. 2(c)) is mainly driven by the heat which is produced from solar energy by the heating system, where the solar just plays the role of providing heat. The photochemical effect may exist at the same time, but the effect is relatively minor. The third type is photothermal coupling catalysis, where the activity of photothermal catalysis exceeds that of the photocatalysis or thermal catalysis processes by the synergistic effect of the thermochemical and photochemical reactions (Fig. 2(d)). Photothermal catalysis has been the hotspot recently (Fig. 3). As we know, for photocatalysis, electron-hole pairs are produced by the excitation of light in the catalyst, then migrate to the surface of catalysts where the excitated electrons participate in the redox reaction. The catalytic reactions for the thermal and photocatalysis are different which can be distinguished as follows: (i) Their performance obatained from the direct experimental data of temperature curves under light and

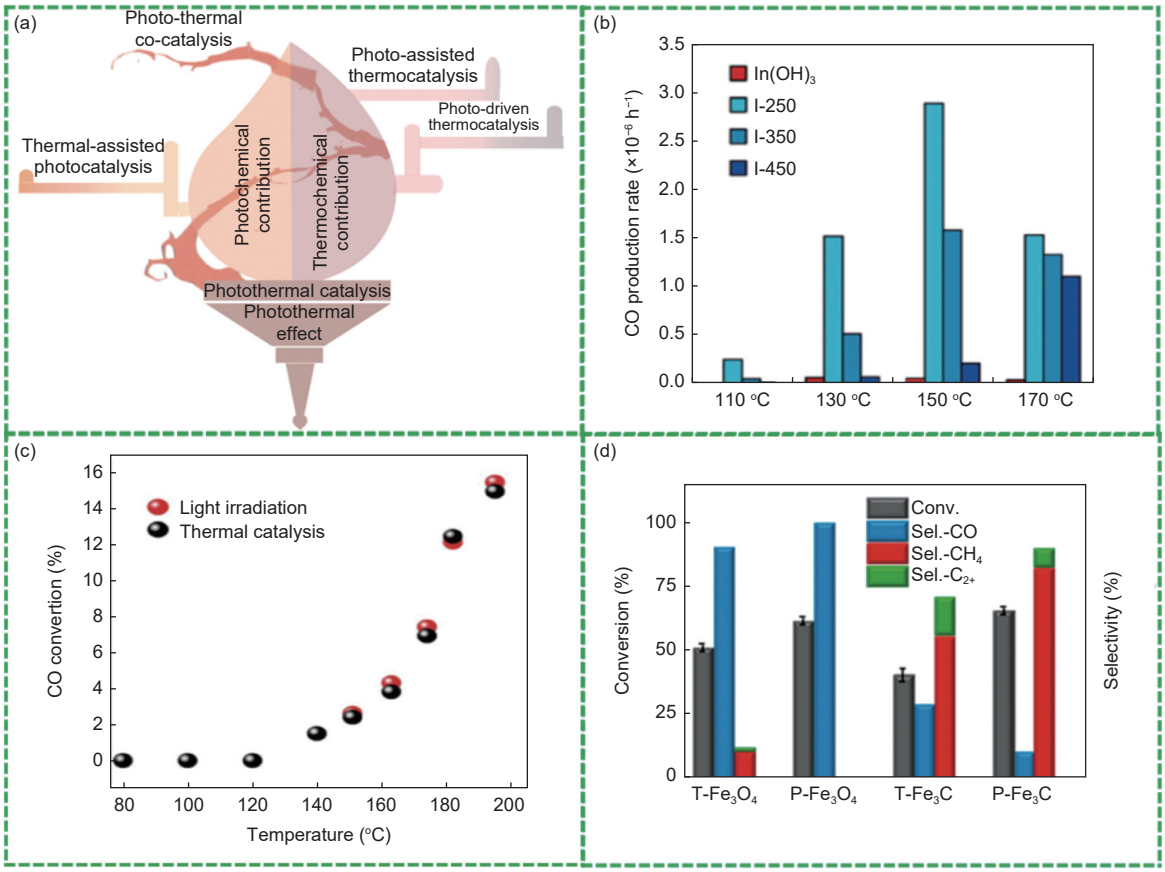

Fig. 2　(a) Functioning principles and categories of photothermal catalysis. Copyright 2021 Elsevier Ltd. (b) Thermal-assisted photocatalysis. Copyright 2014 the authors. Published by Wiley-VCH Verlag GmbH & Co. KGaA, Weinheim. (c) Photo-driven thermal catalysis. Copyright 2018 Wiley-VCH Verlag GmbH & Co. KGaA, Weinheim. (d) Photothermal co-catalysis. Copyright 2020 American Chemical Society

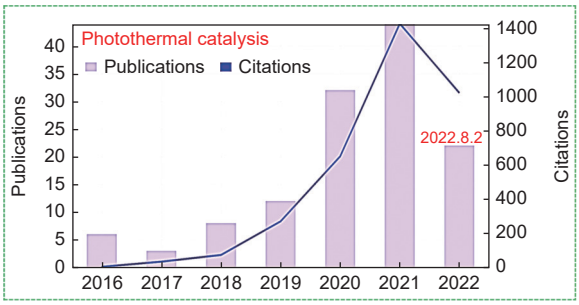

Fig. 3 Total number of publications and citations on the topic over the past decade. The plot was created based on entries in the "Web of Science" (2 August 2022) by using the keywords "CO_2 reduction" and "photothermal catalysis"

dark reaction conditions are different. It is supposed that the selectivity and the production form photocatalysis and thermal catalysis are of the same value at the condition of the same temperature, where light may only produce heat and ultraviolet light may not even be utilized. The difference is evident between the two catalysis pathways caused by the light and thermal effects. (ii) Many issues have been proposed on the accurate measuring of the surface temperature of catalysts. Thermocouples and other measurements do not reflect the local temperature of nanoparticles accurately. It is necessary to calculate the activation energy and the photon utilization rate[15].

2.3 Principle of photothermal catalysis

The typical process of photothermal catalytic CO_2 reduction includes five steps: (i) The catalyst absorbs photons to create electron-hole pairs. When incident light strikes the photocatalyst, the photon energy must be greater than the band gap, and the excited electrons jump to the conduction band (CB) from the valence band (VB), leaving an equal number of holes in the valence band (VB). Then CO_2 molecules adsorbed on the surface of the photocatalyst are therefore reduced by photogenerated electrons. (ii) After electrons and holes are created, they separate and migrate to the surface of the material. The separation process competes directly with charge recombination. The advantage of charge separation over recombination depends on the parameters of carrier lifetime, recombination rate, crystallinity, catalyst size, and surface properties of materials[16]. (iii) The process of carbon dioxide adsorption activation is a prerequisite for electron transfer from catalyst to carbon dioxide molecule. CO_2 is a stable linear symmetrical triatomic molecule, and abundant research achievements have been obtained in its adsorption and activation. In the interaction between CO_2 and catalyst, electrons are injected into CO_2 molecules, leading to the bending of their molecular structure. Bent CO_2 molecules can undergo decomposition, oxidation, or disproportionation reactions. CO_2 is adsorbed on the surface of the catalyst in two forms: The coordination of C and O can form a variety of intermediates such as carbonate, which promotes the activation and reduction of CO_2 molecules. At present, some researchers use catalysts with high specific surface area, such as graphene, whose rich surface could provide abundant active sites for CO_2 molecule adsorption. Another process to improve CO_2 adsorption is to modify the surface of the photocatalyst with alkali metal oxides. The enhanced alkalinity of the catalyst's surface could facilitate CO_2 adsorption. (iv) To promote the redox reactions, the photocatalyst should have an appropriate band gap. The conduction band potential of the catalyst should be higher than that of CO_2, so their conduction band potential is more negative than the surface electron acceptor potential[17]. CO_2 obtains one electron to produce CO_2^- with a reduction potential of −1.9 V (corresponding to standard hydrogen electrode, pH = 7)[18], and two electrons to produce CO or HCOOH with a reduction potential of −0.53 V and −0.61 V, respectively. The remaining reduction products and reduction potentials associated with 4, 6 and 8 electrons are shown in Table 1[19,20]. Where E is the energy absorbed or released during the reaction. On the one hand, the band gap has to be wide because the overpotential is related to these two-electron electrochemical reactions. On the other hand, the band gap of a photocatalyst shouldn't be too wide, as this would limit its efficient use of sunlight. (v) After the photothermal catalytic reaction is completed, desorption of reaction products is very important. If the product couldn't be released from the surface of the catalyst in time, the catalyst would be inactivated[21].

Table 1　Lists the electrochemical CO_2 reduction potentials versus the NHE at pH=7

Reactions	*E* (V *vs* NHE, pH=7)
$CO_2+e^- \rightarrow *CO_2$	−1.9 V
$CO_2+2H^+ +2e^- \rightarrow HCOOH$	−0.61 V
$CO_2+2H^+ +2e^- \rightarrow CO+H_2O$	−0.53 V
$CO_2+4H^+ +4e^- \rightarrow HCHO+H_2O$	−0.48 V
$CO_2+6H^+ +6e^- \rightarrow CH_3OH+H_2O$	−0.38 V
$CO_2+8H^+ +8e^- \rightarrow CH_4+2H_2O$	−0.24 V
$H_2O+2e^- \rightarrow H_2$	−0.41 V

3　Catalysts

The catalyst is the core part of photothermal catalysis, which directly determines the performance of catalysis. As shown in Fig. 4, to obtain an excellent catalyst, it is necessary to choose the right material, because different materials have different catalytic capacities. Further, to obtain higher performance, the structure of the material should be optimized according to the relationship between structure and performance. Finally, the reaction products are also different from the different catalysts, so the catalyst should be selected according to the target product.

3.1　Classification of catalysts

A catalyst is one of the determinants of the photothermal catalysis in the reduction process of CO_2. Exploit the catalysts with high conversion and selectivity is still the key target in CO_2 catalytic conversion[22]. At present, the catalysts used for CO_2 catalytic conversion are mainly noble metal catalysts (Au, Ag) and some transition metal catalysts (such as oxides, metal sulfides, etc.), while some novel catalysts (new carbon materials, MOF materials, layered double hydroxide, etc.) also have good catalytic activity, as shown in Table 2.

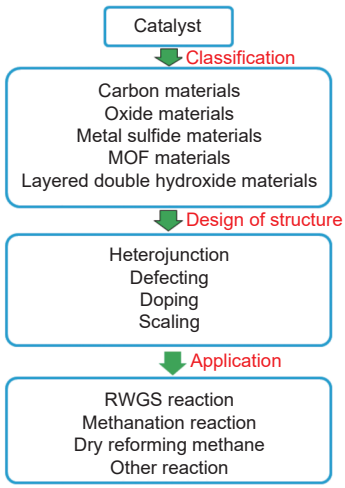

Fig. 4　Preparation of catalyst from the classification of catalyst, design of structure and application

3.1.1　New carbon materials

Carbon materials have the advantages of low cost, easy access, and environmental friendliness, and are widely used in the field of catalysis. Graphite phase carbon nitride (g-C_3N_4) is a new kind of carbon material, which is formed by the sp^2 hybridization of single atoms of carbon and nitrogen. The g-C_3N_4 shows a two-dimensional layered structure. Due to the particularity of electronic structure, g-C_3N_4 can maintain high stability even under acid-base conditions, which could be applied to the photothermal catalytic reduction of CO_2. In addition, the g-C_3N_4 is composed of two common non-metallic elements, C and N[65]. Because of these outstanding features, the research and application of g-C_3N_4 photocatalysts increase rapidly. However, g-C_3N_4 has relatively obvious disadvantages, such as low specific surface area, easy recombination of electron-hole pairs, and low quantum efficiency, which greatly limits its applications. To solve these problems, Bai et al. prepared mesoscopic g-C_3N_4 with a high specific surface area for photothermal catalytic reduction of CO_2[66] (Fig. 5 (a-b)). The yields of H_2, CO and C_2H_5OH are 2.3, 0.7 and 4.0 $mol \cdot g^{-1} \cdot h^{-1}$, respectively. The selectivity strongly depends on the shape of Pd nanocrystals (Fig. 5 (c-d)). After element doping, electrons are transferred from the metal to adjacent N or C atoms. Thus, changing the electron density of N or C atoms could affect the electronic structure and energy band positions of g-C_3N_4. Ma et al. also covalently grafted a Co quaterpyridine molecular complex to semiconductive mesoporous graphitic carbon nitride (mpg-C_3N_4) *via* amide bonds to prepare hybrid catalytic materials[67] (Fig. 5e). It is a selective catalyst for CO in acetonitrile with a high selectivity of 97% while exhibiting remarkable stability with no degradation after 4 days of irradiation (Fig. 5 (f-g)). The above strategies indicate that g-C_3N_4 has superior catalysis properties and would be excellent potential applications in photothermal catalysis.

Table 2 Performance of catalyst materials for photothermal reduction reaction of CO_2

Photothermalcatalysts	Test conditions	Yield (CO) μmol·g^{-1}·h^{-1}	Yield (CH_4) μmol·g^{-1}·h^{-1}	Yield (others) μmol·g^{-1}·h^{-1}	Ref.
	Carbon materials				
gC_3N_4/ graphdiyne	CO_2 and H_2O under 300 W Xe lamp	23.95	0.40	—	[23]
TiO_2/ graphdiyne	CO_2, H_2O and MeCN under 350 W Xe lamp	50.53	2.80	—	[24]
Bi_2WO_6/ Ti_3C_2	CO_2 and H_2O under 300 W Xe lamp	—	1.78	CH_3OH: 0.44	[25]
gC_3N_4/Ti_3C_2	CO_2 and H_2O under 300 W Xe lamp with 420 nm filter	2.42	0.04	—	[26]
$gC_3N_4/Ti_3C_2T_x$	CO_2 and H_2O under 300 W Xe lamp	—	2.12	—	[27]
TiO_2/Ti_3C_2	CO_2 and H_2O under 300 W Xe lamp	—	4.40	—	[28]
$P25/Ti_3C_2$	CO_2 and H_2O under 300 W Xe lamp	11.74	16.61	—	[29]
ZnO/Ti_3C_2	CO_2 and H_2O under 300 W Xe lamp	30.30	20.33	—	[30]
Ni/Nb_2C	CO_2 and H_2O under 300 W Xe lamp	—	72.50	—	[31]
$gC_3N_4/TiO_2/Ti_3AlC_2$	CO_2 and H_2O under 35 WHID car lamp of 20 mW/cm^2 in fixed bed reactor	297.26	2103.50	—	[32]
TiO_2-graphene	300 W Xe lamp, UV- visible light	2.00	25.00	—	[33]
	Oxide materials				
$LaNi_xCo_{1-x}O_3$	300 W Xe lamp equipped with a UV-light filter (λ>420 nm); 350 °C	—	113.13	CH_3OH: 3.47	[34]
Pd-TiO_2	A mercury lamp (500 W, λ>254 nm); 773 K	11.05	—	—	[35]
Ni/TiO_2-CeO_2	300 W Xenon arc lamp, UV light; λ>254	—	17.00	—	[36]
Ni(5)-$BaTiO_3$	300 W Xe lamp, UV–visible light	—	103.70	—	[37]
m-WO_{3-x}	300 W high-pressure Xe lamp (λ>420 nm); 250 °C	—	25.77	CH_3OH: 4.1	[38]
CuS/TiO_2	300 W Xe lamp, UV- visible light; 99 °C	25.97	—	—	[39]
(P-R)Ni/TiO_2	300 W Xe lamp, UV- visible light; 400 °C	—	60 mL	—	[40]
TiO_2/H_2-150	300 W Xe lamp, UV- visible light; 120 °C	23.00	—	—	[41]
CoO-CuO/TiO_2-CeO_2	300 W Xe lamp, UV- visible light; 80 °C	5.00	0.50	—	[42]
$BaZr_{0.5}Ce_{0.3}Y_{0.2}O_{3-\delta}$	300 W Xe lamp, UV- visible light; 350 °C	—	39.13	C_2H_6: 8.64, C_3H_8: 3.22	[43]
Ru/H_xMoO_{3-y}	300 W Xe lamp, Vis-NIR light; 140 °C	—	20.80	—	[44]
BiO_x/CeO_2	300 W Xe lamp, UV- visible light; 400 °C	31.00	—	—	[45]
Pd_2Cu/P25	300 W Xe lamp, UV- visible light; 150 °C	—	—	CH_3CH_2OH: 41	[46]
Ni/TiO_2	300 W Xe lamp, UV- visible light	1.40	271.90	—	[47]
	Metal sulfides materials				
CdS/ graphdiyne	CO_2 and H_2O under 300 W Xe lamp of 100 W·cm^{-2} with AM1.5	16.61	0.32	CH_3OH: 1.79	[48]
SnS_2	CO_2 and H_2O under 300 W Xe lamp of 100 W·cm^{-2} with AM1.5	12.28	—	—	[49]
$ZnIn_2S_4$-In_2O_3	CO_2 and H_2O under 300 W Xe lamp of 100 W·cm^{-2} with AM1.5	3075	—	—	[50]
In_2S_3-$CdIn_2S_4$	300 W Xe lamp, UV- visible light	825	—	—	[51]
CdSe/CdS	300 W Xe lamp, UV- visible light	412.80	—	—	[2]
	MOF materials and derivatives				
(MOF-253–Ru(CO)$_2$Cl$_2$	300 W Xe lamp, UV- visible light	2.73	—	—	[52]
MOFs 1-6	300 W Xe lamp, UV- visible light	4.35	—	—	[53]
TiO_2/C@MOF	300 W Xe lamp, UV- visible light	28.60	—	—	[54]
MOF-525- Co	300 W Xe lamp, UV- visible light	200.60	36.67	—	[55]
UiO-66/CNSS	300 W Xe lamp, UV- visible light	9.00	—	—	[56]
NH_2-MIL-101(Fe)	300 W Xe lamp, UV- visible light	—	—	HCOO: 178	[57]
Ren-MOF	300 W Xe lamp, UV- visible light	6.37	—	—	[58]
ZIF-67	300 W Xe lamp, UV- visible light	37.40	—	—	[59]
	Layered double hydroxide materials				
Co-Co LDHs/$Ti_3C_2T_x$	CO_2, MeCN/H_2O/TEOA and [Ru(bpy)$_3$]Cl$_2$ 6H_2O under 5 W LED lamp	1.25×10^4	—	—	[60]
Niln-LDH/In_2S_3	300 W Xe lamp, UV- visible light	88.29		—	[61]
Ni-Zr-Al	300 W Xe lamp, UV- visible light	—	150 mL·g^{-1}·h^{-1}	—	[62]
Mg-Al	300 W Xe lamp, UV- visible light; 350 °C	12.60	—	—	[63]
NiAl-LDH/CdS	300 W Xe lamp, UV- visible light	12.45	—	—	[64]

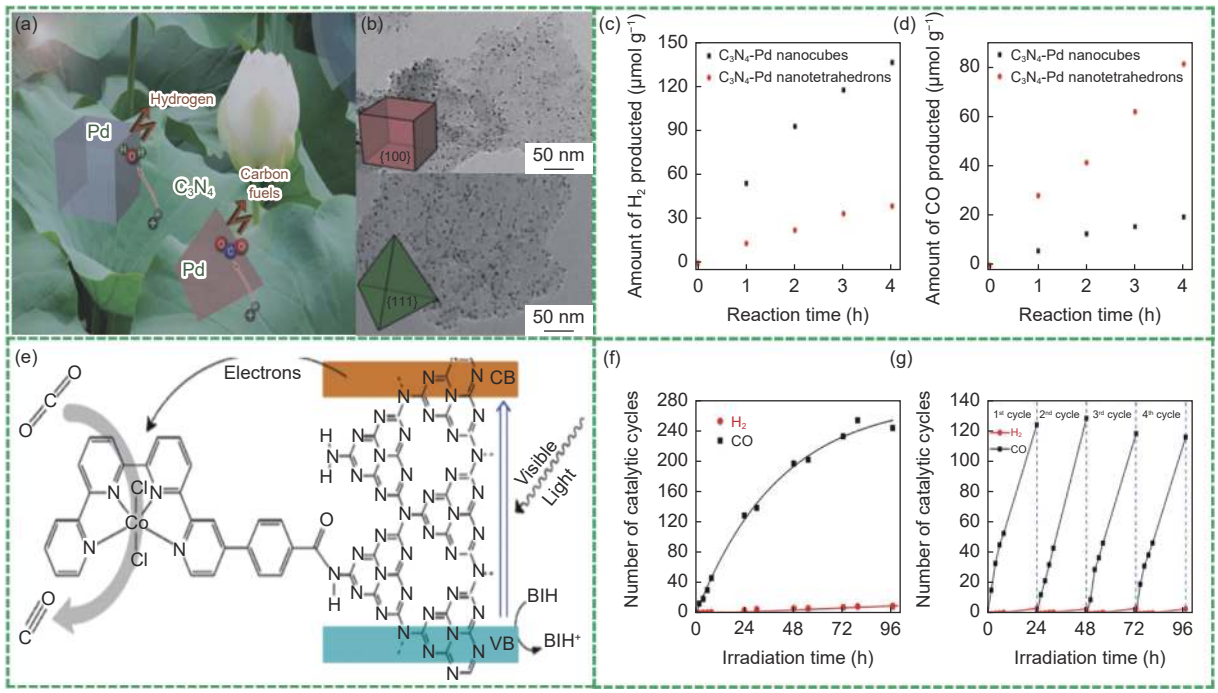

Fig. 5　(a) Schematic diagram. (b) TEM images of g-C_3N_4-Pd nano-cubes (NCs) with Pd(100) facets and g-C_3N_4-Pd nano-tetrahedrons (NTs) with Pd(111) facets. Copyright the Royal Society of Chemistry 2014. (c) H_2 and (d) CO production as a function of reaction time over the sample of g-C_3N_4-Pdnanocubes and g-C_3N_4-Pd nano-tetrahedrons under visible light irradiation. Copyright the Royal Society of Chemistry 2014. (e) Illustration of the visible-light-driven CO_2 to CO reduction process (BIH is the sacrificial electron donor). (f) Generation of CO (black squares) and H_2 (red circles) over 4 days upon visible-light irradiation ($\lambda > 400$ nm) of a CO_2-saturated ACN solution containing 6 mg Coqpy@mpg-C_3N_4, 0.05 M BIH (sacrificial donor) and 0.03 mol L^{-1} PhOH (proton source). (g) Generation of CO (black squares) and H_2 (red circles) during four consecutive 24 h irradiation cycles using the same hybrid material. Copyright 2020 American Chemical Society

3.1.2　Oxide materials

Oxide materials are widely used in photothermal catalytic reactions of CO_2 due to their good catalytic activity, high selectivity, and low price. TiO_2 is an important oxide material used for photothermal catalysis. As a model ctalyst for studying photothermal catalysis technology, a variety of catalysts are developed based on TiO_2. Their modification methods and reaction mechanisms are described and demonstrated according to the characteristics of TiO_2. It has the advantages of high photothermal catalytic activity and stability, but its optical response range limits the application range in the ultraviolet region. The effect of TiO_2 crystal structure on the reaction rate has been extensively studied. When the TiO_2 is modified with noble metals, the photogenerated electrons in the noble metal with a higher conduction band position would be transferred to the TiO_2 conduction band, while the photogenerated holes would remain in the noble metal, which would facilitate the separation of the photogenerated carriers and improve the photocatalytic activity[50]. Neatu et al. modified the TiO_2 film with Au-Cu dual metal centers to reduce CO_2 (Fig. 6 (a-b))[68]. Due to the Au-Cu alloy structure, the maximum production of CH_4 is 2 000 μmol·g^{-1}·h^{-1} (Fig. 6(c)), and the selectivity is up to 97%. Similar to alloy-type oxide material, perovskite-type oxide materials are also widely used in photothermal catalysis. Shan et al. successfully prepared boron-doped layered polyhedron $SrTiO_3$ (STO) by the solid-state method using a specific TiB_2 precursor as a boron and titanium resource[69]. More efficient charge separation of $SrTiO_3$ is achieved by an appropriate amount of B doping[53–55], and the production of CH_4 and CO reach 14 and 21 mol·h^{-1}·g^{-1}, respectively (Fig. 6 (d-f)).

3.1.3　Metal sulfides materials

Metal sulfides have become one of the promising candidate catalysts for CO_2 reduction due to their abundant reserves, good light absorption properties, low cost, and friendly preparation processes. Des-

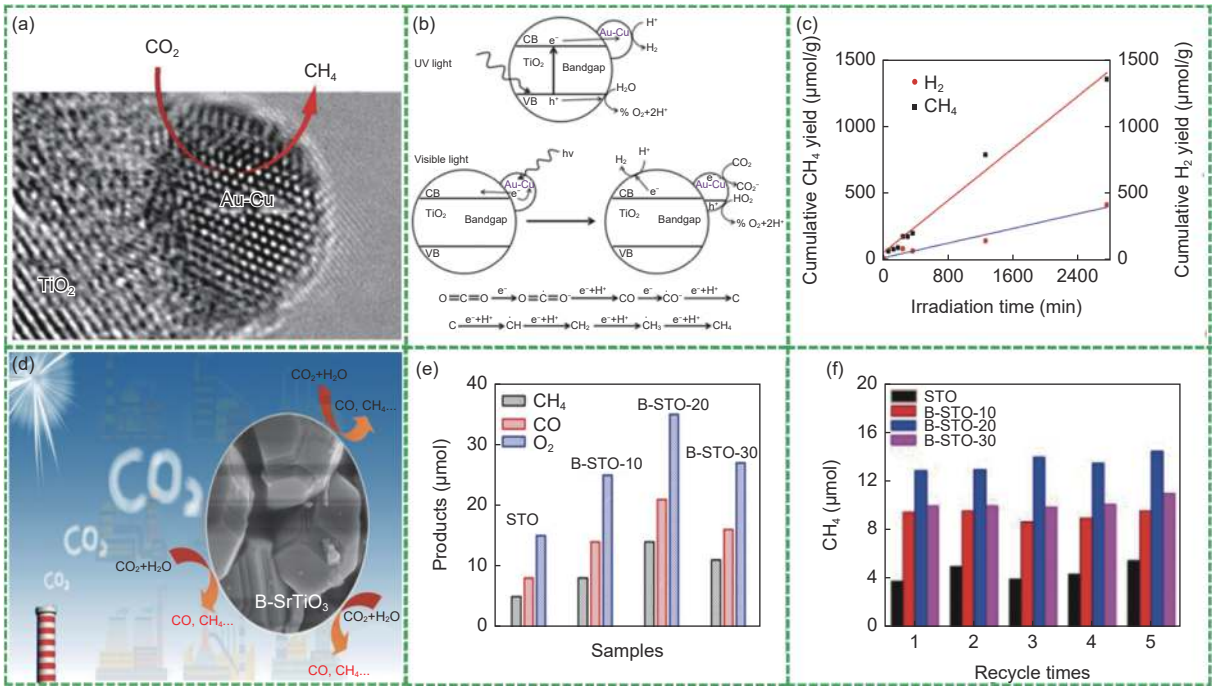

Fig. 6 (a) HRTEM image of Au-Cu/TiO_2 material. (b)The top part summarizes the proposal to rationalize the influence of the irradiation wavelength range on the product distribution using (Au, Cu)/TiO_2 as photocatalysts. The bottom part presents a plausible route for methane generation in the gas-phase CO_2 photoreduction by water. (c) Temporal evolution of H_2 and CH_4 production throughout 46 h of irradiation time using (Au, Cu)/TiO_2 (Au/Cu ratio 1∶2). Copyright 2014 American Chemical Society. (d) Graphical abstract. (e-f) The production rates of CH_4 during the photocatalytic CO_2 reduction with H_2O on STO, B-STO-10, B-STO-20, and B-STO-30. Copyright 2017 Elsevier Ltd

pite the above advantages, the efficiency of metal sulfides is still relatively low due to the sluggish carrier separation and migration kinetics for photoreduction CO_2. Combining two metal sulfides with suitable band gaps is one of the promising strategies to enhance the performance of catalysts. Zhang et al. utilized a novel sulfur-mediated and Co-NCPs-derived self-templated strategy to synthesize yolk-shelled $CdS/CdCo_3$-CoS_2 composite[70]. The prepared hierarchical nanotubes could promote the separation and migration of photogenerated charge carriers, improve the adsorption of CO_2 molecules, and provide abundant active sites[57]. Semiconductor quantum dots (QDs) have the advantages of low cost, easy preparation, strong visible light harvesting ability, easy control of charge carriers, and abundant surface sites. Guo et al. presented the first example of combining solar-driven organic oxidation reactions with CO_2 reduction, making full use of excited electrons and holes to generate high-value-added organic chemicals while generating solar fuel $(CO)^2$ (Fig. 7 (a)). Under visible light, the photogenerated electrons of CdSe/CdS QDs could convert CO_2 to CO and the holes could oxidize triethylamine. The CO formation rate can be as high as ~412.8 $mmol \cdot g^{-1} \cdot h^{-1}$ and selectivity as high as ~96.5%. The turnover number (TON) and apparent quantum efficiency (AQY) of the system under illumination for 1.0 h are as high as ~47 360 $mmol \cdot g^{-1} \cdot h^{-1}$ and 32.7%, respectively (Fig. 7 (b-f)). The change of quantum dots size could regulate their absorption spectrum region to reach an excellent performance.

3.1.4 MOF materials and derivatives

Metal-organic frameworks (MOF) materials have been applied to photothermal catalysis due to their large specific surface areas, adjustable porosities, and topological diversities. As photocatalysts, MOFs have the following characteristics: (i) MOFs can be obtained by screening different organic ligands and metal elements, which determines their rich species and diverse structures. (ii) They could promote the separation and transfer of charge and inhibit the recombination of electrons and holes by changing the crystal structure, to effectively improve sunlight absorption

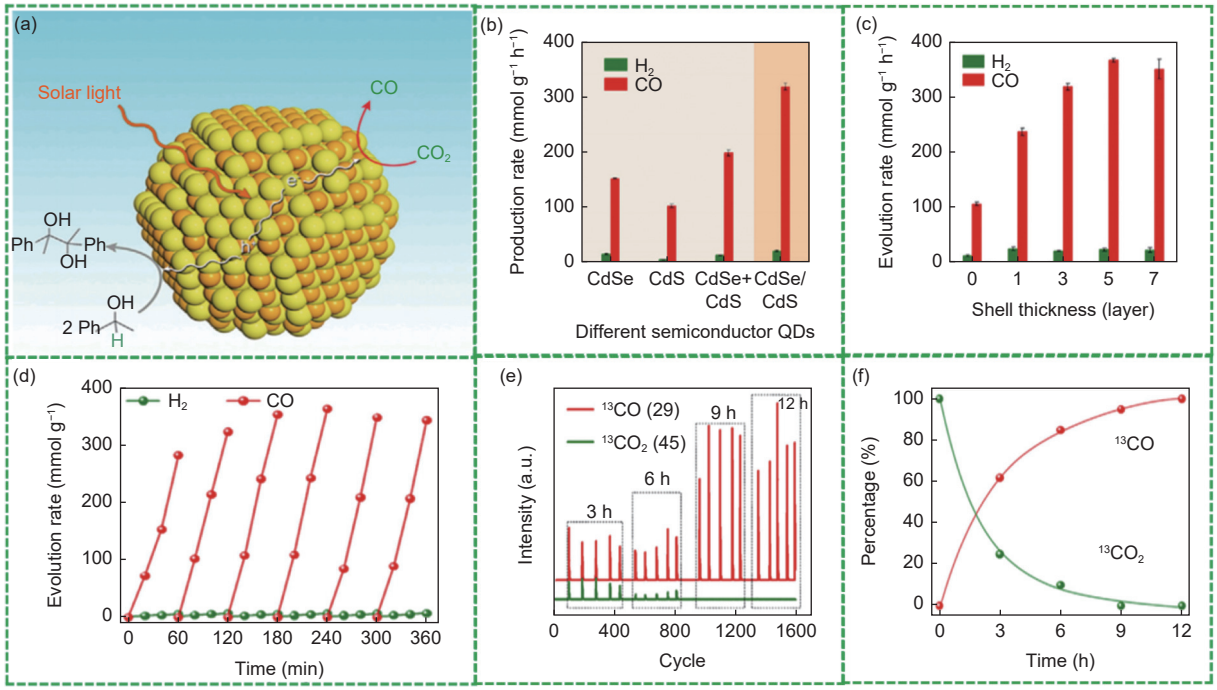

Fig. 7　(a) Photocatalytic CO_2 reduction coupled with oxidative organic synthesis by semiconductor QDs. (b)The rate of photocatalytic CO_2 reduction reaction using different semiconductor QDs as the photocatalysts. (c) Photocatalytic CO_2 reduction of CdSe QDs modified with a different atomic thickness of CdS shell under the same conditions. (d) Long-time photocatalytic CO_2 reduction experiment using CdSe/CdS QDs as photocatalysts and TEA as an electron donor under Xe lamp irradiation (300 mW with 400 nm filter). (e) GC-MS chromatogram of gas products obtained by photocatalytic reaction under CO_2 atmosphere with different irradiation times. (f) Growth kinetics of CO and the corresponding decay kinetics of CO_2 along with 450 nm LEDs irradiation obtained from GC quantization. Copyright 2019 Elsevier Inc

and utilization efficiency. (iii) The large specific surface areas of MOFs bring benefits to the adsorption of substrate molecules around their active sites[71], which is excellent activation and catalytic conversion. Recently, porphyrins or metal porphyrins have gained attention because of their high photo-capture efficiency and pho-catalytic activity. Xu et al. found that PCN-222 (MOF-545) could selectively capture CO_2 (Fig. 8(a))[72]. Furthermore, PCN-222 shows significant photothermal catalytic activity with a long light time, and the amount of $HCOO^-$ could reach 30 μmol after 10 h reaction (Fig. 8(b)). For the organic ligand modification, the NH_2 functional group modification could notably enhance the photocatalytic efficiency of MOFs. The reason is that the -NH_2 group has a high affinity for CO_2, which is favorable to the enhanced adsorption capacity[73]. Usually, the MOFs are unstable in the water. The UiO series is based on the structural unit of $Zr_6O_4(OH)_4(CO_2)_{12}$ and the dicarboxylic acid ligand is highly stable in water. Wang et al. obtained MOF-4 by introducing the H_2L_1-H_2L_6 into the stable UiO-67, which catalyzes CO_2 reduction under visible light[53] (Fig. 8(c)). The performance test shows that when the reaction time is increased to 2 h, the catalytic activity of MOF-4 would be higher than that of H_2L_4, and can maintain good stability (Fig. 8(d)). H_2L_4 is prone to compound between photogenerated electrons and holes under a long-time reaction, and the special crystal structure of MOF is conducive to the separation of photogenerated electrons and holes, further enhancing the photothermal catalytic activity and CO_2 reduction efficiency.

3.1.5　Layered double hydroxide materials

Layered double hydroxide (LDHs) is a special type of layered material. This layered material is composed of several layers of positive charge layers and anions in the middle[74]. Layered double hydroxides are a class of layered double metal hydroxides, which are considered to be ideal photocatalysts. Chen et al. successfully prepared a series of novel CoFe-based catalysts by utilizing the hydrogen reduction process

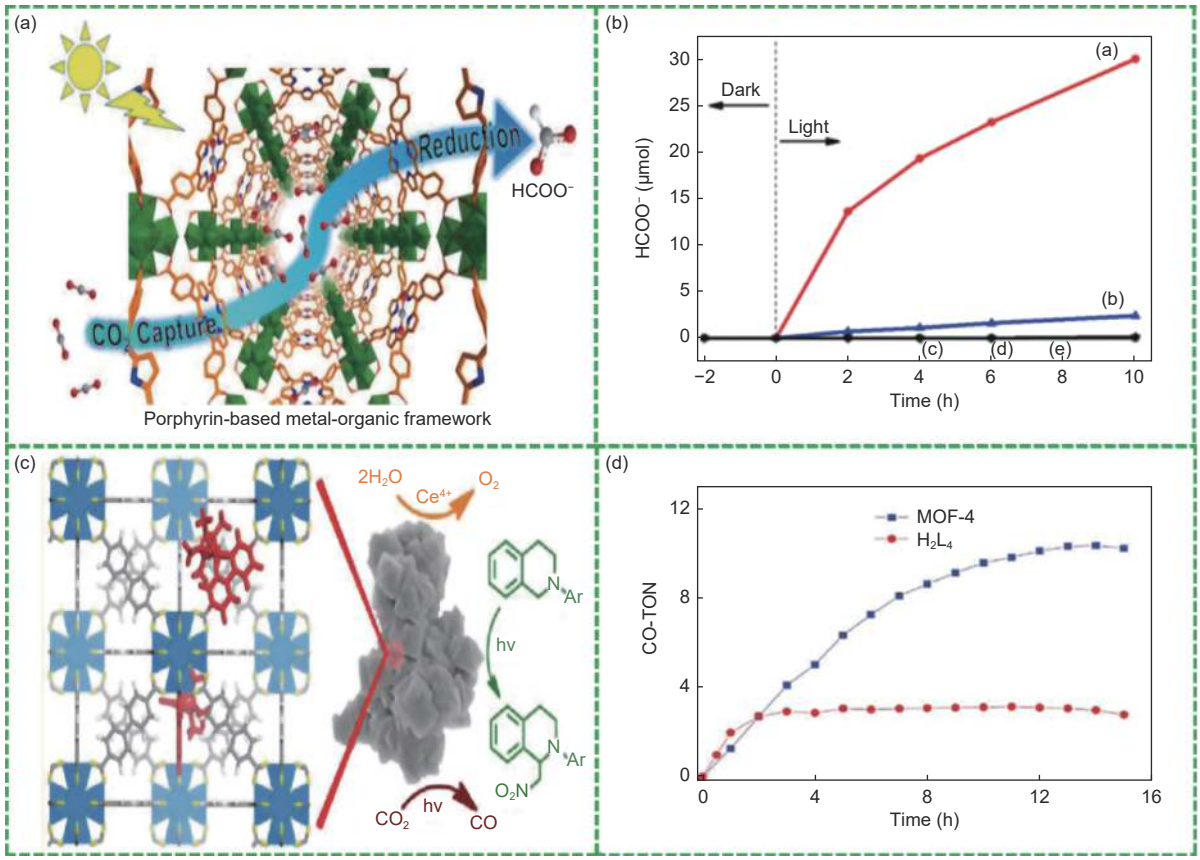

Fig. 8 (a) Schematic diagram. (b) The amount of $HCOO^-$ produced as a function of the time of visible-light irradiation. Copyright 2015 American Chemical Society. (c) Schematic diagram. (d) Plots of CO evolution turnover number CO-TON versus time in the photocatalytic CO_2 reduction with MOF-4 (blue square) and homogeneous H_2L_4 (red circle). Copyright 2011 American Chemical Society

of CoFeAl LDH nanosheets at 300-700 °C[75] (Fig. 9(a)). Because of the large specific surface area, nano-sheet morphology provides abundant active sites for the catalytic reaction. CoFe-650 LDH nanosheets exhibit outstanding selectivity to carbon-based chemicals (60% methane, 35% C_{2+}) (Fig. 9 (b, c)).

3.2 Strategies and factors tuning catalytic activity

Usually, when the performance of the catalyst cannot meet the needs of people or people who pursue a particular reaction, the catalyst needs to be optimized to achieve specific purposes. The factors such as crystal structure, crystal surface[76], specific surface area, morphology, surface characteristics, and particle size directly affect the reduction efficiency and product selectivity of the photothermal catalytic CO_2 reduction reaction[77]. To improve the photothermal catalytic efficiency, it is necessary to design catalysts with special functions according to the properties of the materials. Several key factors need to be considered in the design process of catalytic materials: (i) The catalyst should have a large light absorption range and use solar energy efficiently. (ii) The catalytic material should reduce the recombination of electron-hole pairs as much as possible and shorten the distance between electron-hole pairs to the surface of the catalyst as much as possible. (iii) Catalyts should have enough activated centers to activate inert CO_2 molecules and convert them from linear molecules to bent activated molecules. (iv) Electrons of the conduction band should have high enough energy to promote the reduction of carbon atoms in CO_2 molecules, and the holes in the valence band should have sufficient capacity to oxidize water. Based on the above criteria, we summarize some commonly methods to regulate the surface properties of catalysts (Fig. 10).

3.2.1 Heterojunction

Different morphological structures of catalysts have great impacts on the performance of CO_2 reduc-

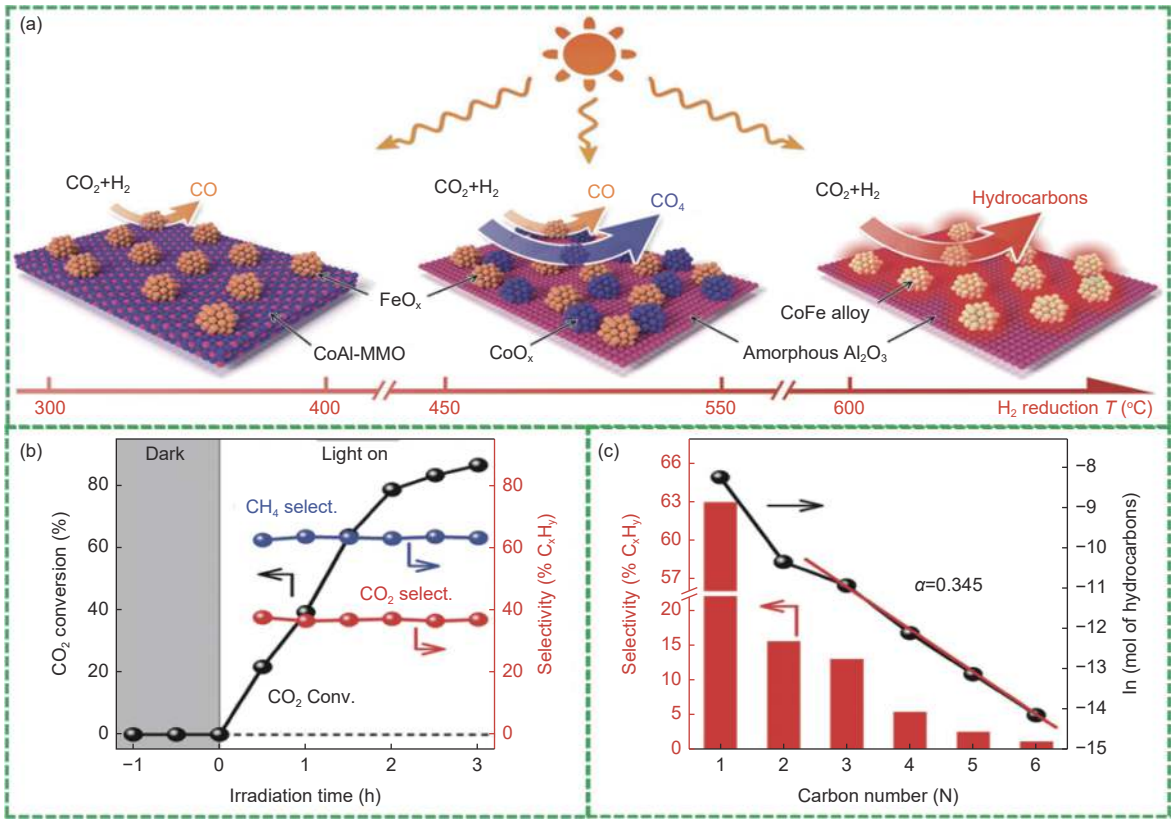

Fig. 9　(a) Illustration of the different CoFe-x catalysts formed by hydrogen reduction of a CoFeAl-LDH nanosheet precursor at different temperatures. (b) Time course of CO_2 conversion and product selectivity for CO_2 hydrogenation over CoFe-650 under UV–vis irradiation. (c) The hydrocarbon product distribution was obtained over CoFe-650 under UV–vis irradiation for 2 h. Copyright 2017 WILEY-VCH Verlag GmbH & Co. KGaA, Weinheim

tion[78–79]. A reasonable structure could promote the separation of photogenerated electron-hole pairs or shorten the transport distance of electron-hole pairs, reduce the probability of electron and hole recombination, and improve the conversion rate of CO_2. According to the difference in band gap width, conduction band, and valence band position (Fig. 11(a))[80], different heterojunctions are designed carefully, which is helpful for photoelectron excitation and electron-hole pair separation. Xu et al. developed a titania/perovskite ($CsPbBr_3$) S-type heterojunction by a simple electrostatically driven self-assembly method (Fig. 11(b))[81]. *In-situ* X-ray photoelectron spectroscopy analysis also reveal that the internal electric field drives photoexcited electron transferring from TiO_2 to $CsPbBr_3$, indicating that a S-type heterojunction is formed in the TiO_2/$CsPbBr_3$ nanohybrid, which greatly facilitates the separation of electrons and holes and promotes the efficiency of carbon dioxide photoreduction. Yan et al. also reported a Bi_4TaO_8Cl/

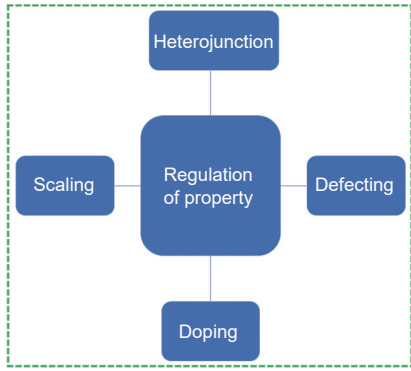

Fig. 10　The methods of regulating material properties

$W_{18}O_{49}$ (BiW) Z-scheme system assembled from Bi_4TaO_8Cl nanosheets and nanoscale $W_{18}O_{49}$ for the photothermal catalytic reduction of CO_2 (Fig. 11(c))[82]. The superior performance of the BiW Z-scheme system at high reaction temperatures is considered to be the thermal shuttle effect of electrons from $W_{18}O_{49}$ to Bi_4TaO_8Cl[83]. Zhang developed a general strategy to covalently link covalent organic frameworks (COFs) to semiconductors to create stable organic-inorganic Z-scheme heterojunctions for artificial photosynthe-

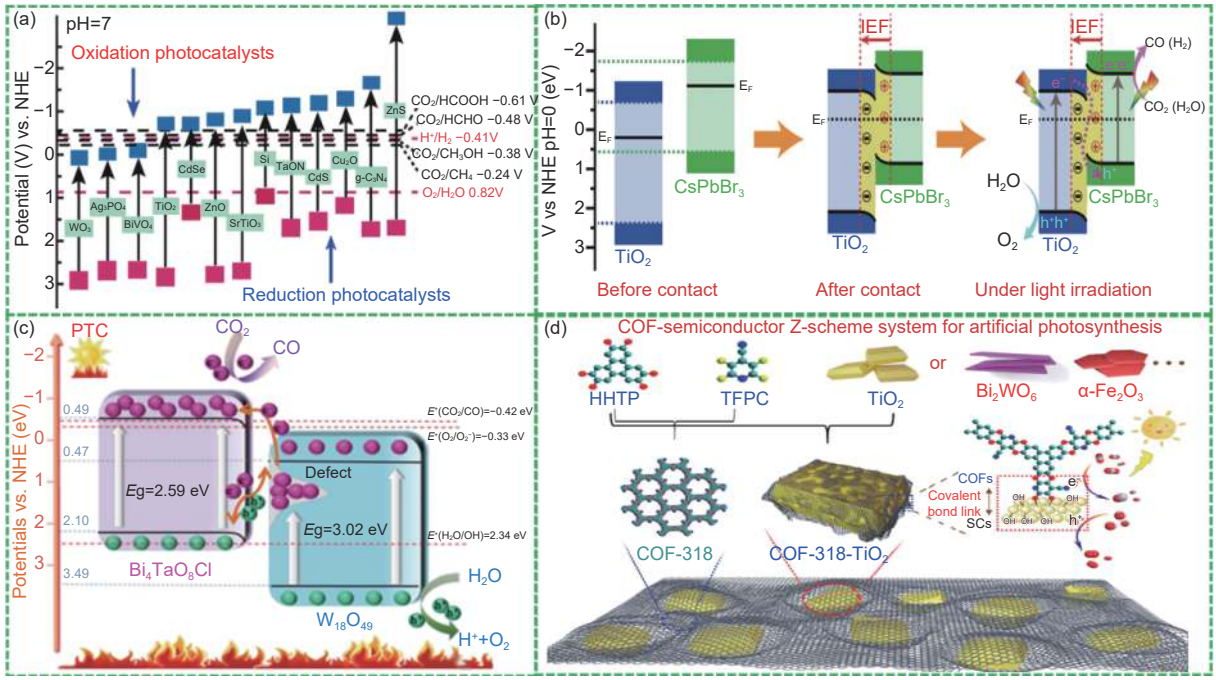

Fig. 11 (a) Band structures of some representative photocatalysts. Copyright 2020 Elsevier Inc. (b) Schematic illustration of TiO_2/$CsPbBr_3$ heterojunction: internal electric field (IEF)-induced charge transfer, separation, and the formation of S-scheme heterojunction under UV–visible-light irradiation for CO_2 photoreduction. Copyright 2020 Springer Nature Inc. (c) Schematics illustrating the photo-excited electron-hole separation process of BiW heterostructures in photothermal catalysis. Copyright 2019 Elsevier Inc. (d) Schematic representation of the preparation of COF-318-SCs via the condensation of COF-318 and semiconductor. Copyright 2020 Wiley-VCH Verlag GmbH & Co. KGaA, Weinheim

sis[84] (Fig. 11(d)). A series of photocatalysts combining semiconductors were synthesized, and water was used as the electron donor for the reduction of carbon dioxide without additional photosensitizers and sacrificial agents. This is the first report that the covalent bond-inorganic semiconductor Z-schemes was applied to artificial photosynthesis.

3.2.2 Defecting

It has been well-acknowledged that defects are the CO_2 adsorption sites. The local electronic environment and optical properties of the catalyst can be well regulated by the controlled introduction of defects. The vacancy could be obtained by removing oxygen, carbon, or nitrogen atoms. In addition, the induced vacancy can effectively capture the thermal electrons, reduce the recombination effect, and achieve longer wavelength light absorption. Ye et al. induced oxygen vacancies in MoO_3 to enhance photothermal CO_2 reduction efficiency by trapping near-infrared photons[85]. The localized surface plasmon resonance (LSPR) of MoO_{3-x} triggered by oxygen vacancies enables the efficient capture of the near-infrared photons (Fig. 12 (a-e)). Yu et al. developed a simple and convenient solution plasma processing (SPP) technique to treat pre-synthesized yellow TiO_2 with abundant oxygen vacancies (O_v) that incorporates hydrogen dopants into TiO_2 crystals[86]. At high temperatures, the SPP-treated TiO_2 exhibits a higher conversion rate for CO_2 reduction than untreated TiO_2 under solar light and a higher removal rate of acetaldehyde under UV light[87] (Fig. 12 (f-i)).

3.2.3 Doping

Doping engineering introduces heteroatoms (metal or nonmetal) while vacancy engineering removes atoms. Doping is a method by introducing the impurity atoms into the lattice structure of the catalyst, causing a change in the electronic structure, moving the position of the valence band and conduction band, and improving the activity of the catalyst. The mechanism of doping can be summarized as follows: (i) By doping, heteroatoms replace the lattice position of the original catalyst and form a new chemical bond. As a result, the catalysts reduce the threshold of light excitation, improve the quantum efficiency, broaden the spectrum response range, and improve the utiliza-

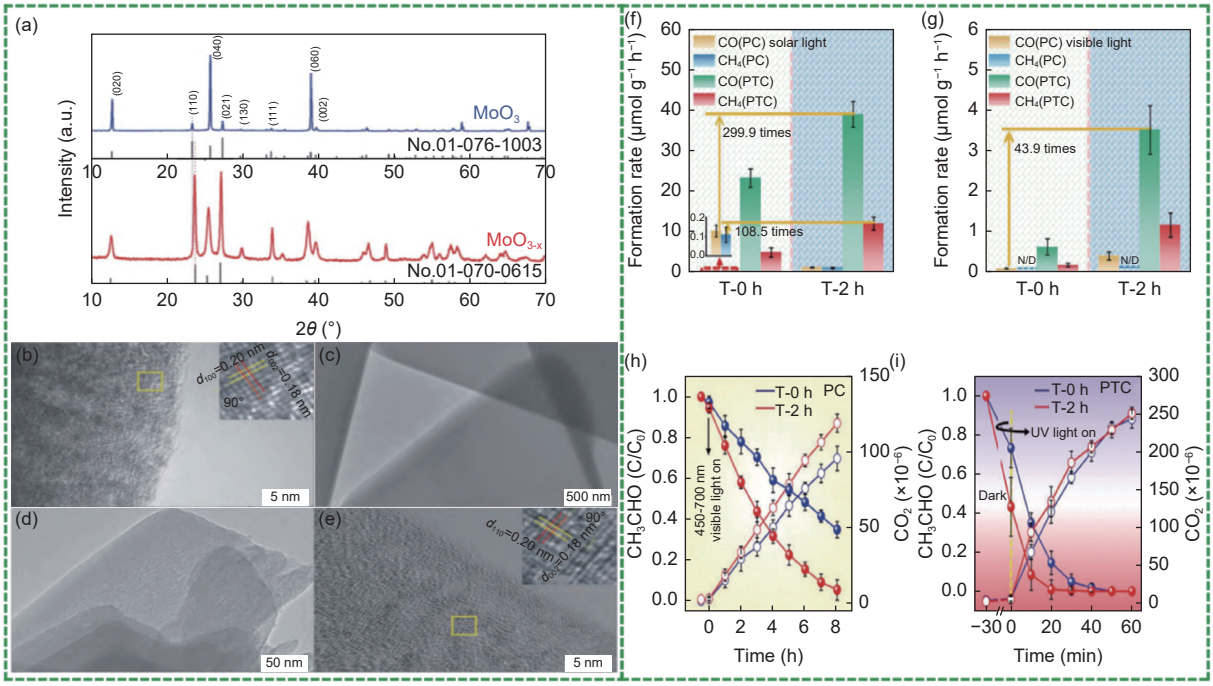

Fig. 12　Crystal structure of MoO_{3-x} and MoO_3: (a) XRD patterns. (b) TEM of the MoO_3. (c) TEM of the MoO_{3-x}. (d) HRTEM of the MoO_3, and (e)HRTEM of the MoO_{3-x}. Copyright the Royal Society of Chemistry 2019. Photothermal catalytic activities of CO_2 conversion over TiO_2(AB) treated with SPP for 0 and 2 h (samples T-0 h and T-2 h, respectively) upon (f) 100 mW·cm^{-2} solar and (g) visible ($\lambda \geqslant 420$ nm) light irradiation (N/D: not detected). Acetaldehyde degradation and CO_2 evolution over T-0 h and T-2 h: (h) under visible light at room temperature and (i) under UV light with heating at 70 °C. Copyright 2020 The Authors Published by WILEY-VCH Verlag GmbH & Co. KGaA, Weinheim

tion rate of photons. (ii) Doping forms doping energy levels, which can regulate the band gap width and improve the redox performance of the catalyst. (iii) The lattice defects increase the conductivity of the catalysts to promote the separation of electron-hole pairs. Liu et al. synthesized Zn and N co-doped porous carbon nanosheets (ZNCs) as photothermal catalysts by a facile one-step pyrolysis method[88] (Fig. 13(a)). The ZNCs exhibit a graphene-like layered architecture and dispersed Lewis acid (Zn atom) sites and Lewis base (N atom) sites, which could realize full-spectrum absorption and excellent photothermal conversion efficiency. Qi et al. also proposed a carbon doping strategy to endow In_2O_3 with favorable surface modifications. Carbon doping could induce the generation of oxygen-rich vacancies[89]. The introduction of oxygen defects and carbon doping in the bandgap of In_2O_3 significantly increase the absorption of sunlight in the full spectrum (Fig. 13(b)). Therefore, carbon-doped In_2O_3 achieves efficient photothermal conversion and a high CO generation rate of 123.6 mmol·g^{-1}·h^{-1} as well as outstanding stability in photothermal catalytic CO_2 reduction (Fig. 13 (d, e)). The surface modification of metal oxide catalysts, including the introduction of oxygen vacancies and loading of metals (Au) or metal oxides (MgO), has a considerable impact on the product selectivity of the CO_2 reduction reaction[90] (Fig. 13(c)). The free energy of the CO_2 reduction reaction on the modified anatase TiO_2 (101) surface is calculated based on density functional theory. The modified surface enhances the competition between the crucial intermediates (CO*, HCOOH*, HCHO* and CH_3OH*)[91], which is essential for the selectivity of CO_2 reduction. The loading of Au and MgO enhances the electron transfer between the key intermediates[39–40], which effectively activates the crucial intermediate and significantly improves the CH_4 selectivity of CO_2 reduction.

3.2.4　Nano-scaling

The size effect is one of the most important factors in the structure-performance relationship of catalysts. Photothermal catalyts from the block materials, the nanoclusters to the single atom, with the de-

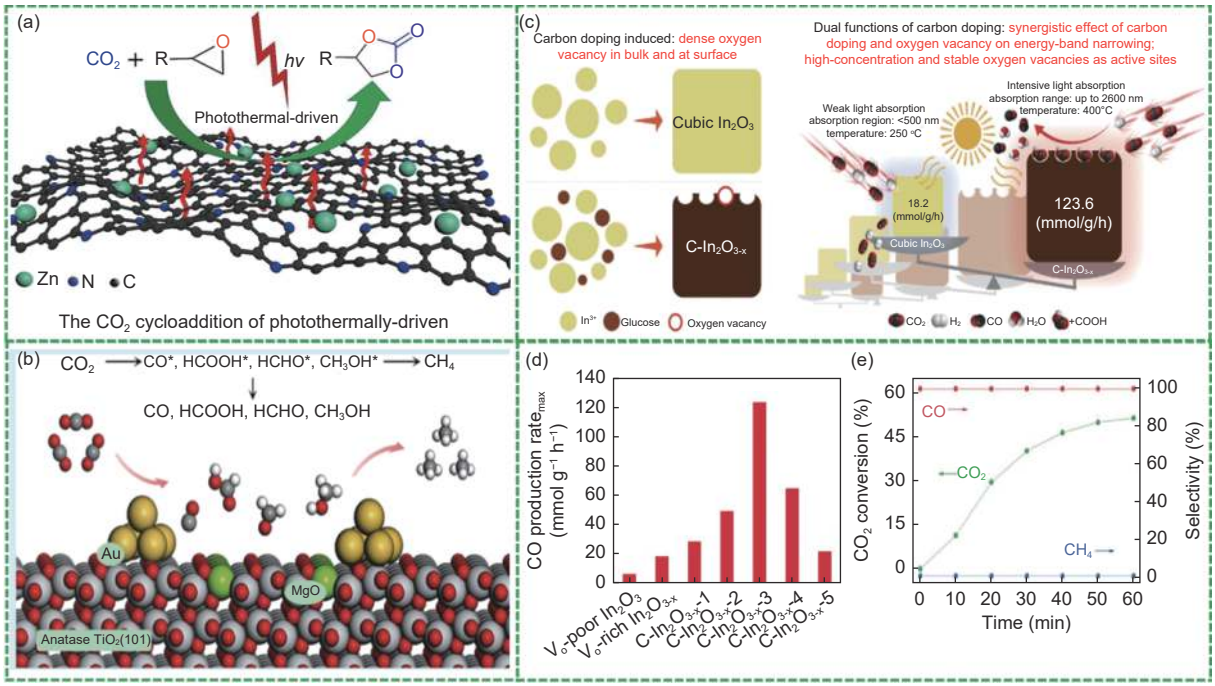

Fig. 13 (a) The CO_2 cycloaddition of photothermally-driven, Copyright 2022 Elsevier Inc. (b) Graphical abstract. Copyright 2021 American Chemical Society. (c) Schematic illustration of the formation mechanism, catalytic process, and advantages for CO_2 photothermal reduction into CO over C-In_2O_{3-x}. (d) CO production rates of Vo-poor In_2O_3, Vo-rich In_2O_{3-x} and C-In_2O_{3-x} with different carbon content. (e) Photothermal CO_2 conversion test and selectivity of C-In_2O_{3-x}. Copyright 2021 Wiley-VCH GmbH

crease of the particle size, their electronic structure, and the geometric structure would change. Because the surface free energy of the catalyst sharply increases, the chemical site of the catalyst becomes more and more, which is easier to adsorb and activate CO_2 molecules. The photothermal catalyst becomes more and more active. For nanoparticles, the "nano effect" of photothermal catalysts has been studied extensively and deeply over the past decades. With the development of novel characterization instruments, people have gradually shifted their attention to a region less than 1 nm[92]. In recent years, it has been slowly realized that when the size of catalysts is reduced below 1 nm, they would exhibit different catalytic behaviors compared with conventional nanoparticles. Liu and Corma discussed the size effect on the electronic and geometric structures of catalysts[93]. For single atom, the electron structure is simple and can be approximated as the corresponding atomic orbital structure[55]. For clusters, they can be regarded as molecular orbitals formed by multiple atoms through hybridization, which is the transition state between a single atom and a nanoparticle (Fig. 14(a)). When the size increases to the nanoparticles, the successive energy level structure is formed. Based on the templated growth and pyrolysis of vacant metal-organic framework precursors, Yang et al. prepared a new class of hollow porous carbons (HPCs) with well-dispersed nitrogen and single zinc atoms[94]. Taking advantage of the ultra-high weight loading of (11.3%) single-atom Zn active sites and dispersed N active sites, HPC realizes the efficient CO_2 cycloaddition reaction under light irradiation. Lee et al. reported a Cu-Pt alloy nanocluster supported by a titania catalyst for the photothermal catalysis CO_2 conversion to methane[95] (Fig. 14 (b, c)). As the size of the Cu-Pt alloy decreases, the photocatalytic activity increases significantly. The small Cu-Pt nanoclusters are tightly bound to the carbon dioxide intermediate and have stronger interactions with titania, which also contribute to the high production rate of methane. Alloying effect and size effect of the catalyst is proved to be the key method to taking an efficient CO_2 reduction reaction (Fig. 14(d)).

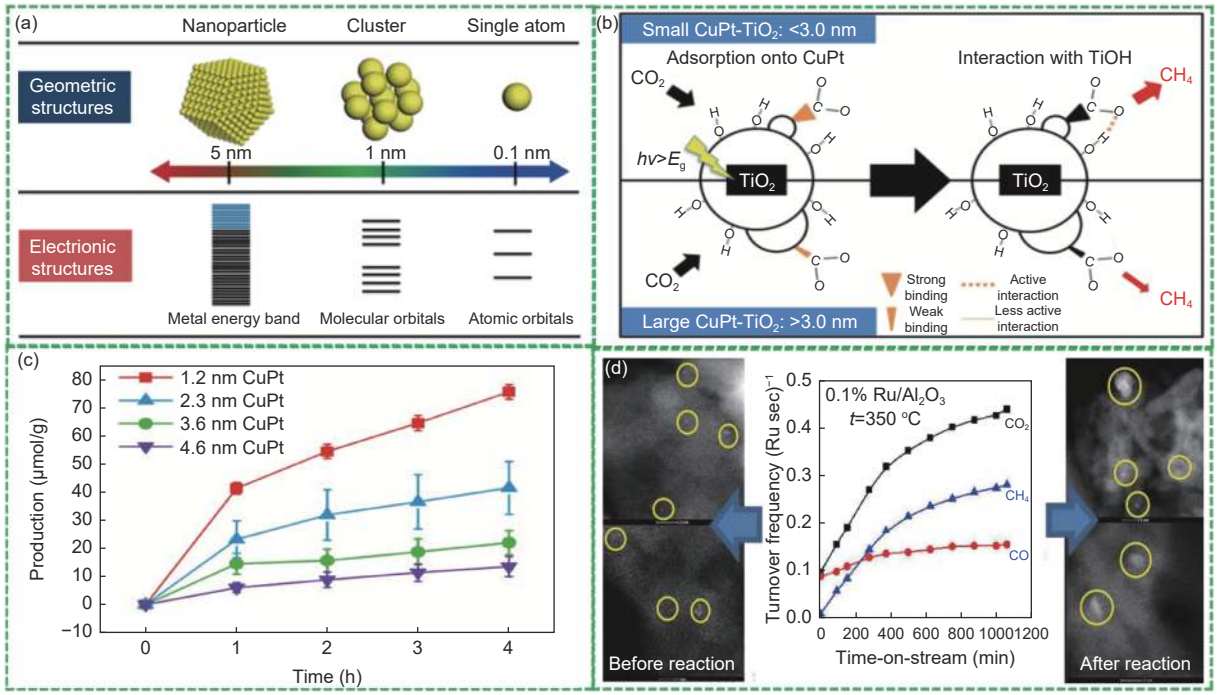

Fig. 14　(a) Geometric and electronic structures of a single atom, clusters, and nanoparticles, Copyright 2018 American Chemical Society. (b) Illustration of CO_2 conversion mechanism on small and large Cu-Pt nanoclusters on TiO_2. (c) Photocatalytic CH_4 evolution as a function of time. Copyright the Royal Society of Chemistry 2013. (d) Schematic diagram. Copyright 2013 American Chemical Society

4　Application of photothermal catalysis

Photothermal catalysis has been applied in many fields, among which the synthesis of high-value-added hydrocarbon is one of them. The product depends on many factors, including the type of catalyst, pressure, temperature, and reactant gas.

4.1　RWGS reaction

RWGS is the reverse water gas shift (WGS) reaction. The reduction reaction transforms CO_2 into CO and CO further synthesizes important chemical products, such as alkanes, alkenes, alcohols, formaldehyde, and formic acid compounds, to realize the C cycle and eventually achieve the goal of zero CO_2 emission[96]. In the RWGS reaction, the oxidation and reduction reactions occur between the surface of the catalyst. Generally, the reaction enthalpy of RWGS is 42.1 kJ mol^{-1}, which is a classical endothermic reaction (Eq. (4)). According to the relevant concepts of thermodynamics, high temperature is more conducive to the direction of CO formation. From the molecular dynamics point of view, high temperature accelerates the reaction rate[97].

$$CO_2 + H_2 \leftrightarrow CO + H_2O \quad \Delta H_{298K} = 41.2\ \text{kJ}\cdot\text{mol}^{-1} \quad (4)$$

RWGS reaction follows two typical reaction paths[98]: (i) The redox mechanism. CO_2 dissociates on the surface of the catalyst as CO and O*, and then H_2 reacts with O*. According to the redox mechanism, the binding strength of CO* on the surface of catalyst particles can determine product selectivity. The strong interaction between CO* and catalyst particles leads to the dissociation of the C═O bond, which is conducive to the formation of CO. Therefore, regulating the adsorption strength of CO* on the catalyst surface could highly improve the CO selectivity in reverse water gas reactions. (ii) Intermediates mechanism, H_2 and CO_2 directly react on the surface of the catalyst to produce intermediates (such as carboxylate or bicarbonate, etc.), and further hydrogenate to CO and H_2O. According to the intermediate-product mechanism, intermediates only form at the surface of catalyst particles, and hydrogen atoms adsorbed on catalyst particles could further react with intermediates. After the reaction, CO and H_2O are desorbed. Lu et al. reported an Au/CeO_2 catalyst for photothermal inverse water gas shift, achieving high conversion and high CO selectivity[99] (Fig. 15 (a, b)). *In-situ* infrared spec-

troscopy and kinetic experimental results indicate that the special effect of light relates to the promotion of hydrogen decomposition (Fig. 15 (c, d)). The robust Au/CeO_2 catalyst displays excellent activity and CO selectivity for CO_2 reduction under long-term light irradiation. Furthermore, the photothermal reaction rate is much higher (>10 times) than that of being carried out under thermal conditions (Fig. 15 (e, f)).

4.2 Methanation reaction

Elucdating the reaction pathway helps us understand the reaction mechanism and design catalysts with adsorption sites. The methanation pathway may be related to the reaction conditions (temperature, pressure, etc.) and the surface properties of the catalyst (hydroxyl richness, CO_2 adsorption sites). The change in the reaction pathway could affect the selectivity of the product. There are two reaction pathways: the formaldehyde pathway and the carbene pathway. There are multiple intermediates in the formaldehyde reaction pathway[100–101], $CO_2 \rightarrow HCOOH \rightarrow H_2CO \rightarrow CH_3OH \rightarrow CH_4$. The reduction of CO_2 firstly obtains HCOOH through gaining two-electron and hydrogenation reaction and then continues to gain electrons to generate H_2CO and CH_3OH. H_2CO and CH_3OH are intermediates rather than by-products. The selection of the two intermediates is affected by the adsorption force on the surface of the catalyst. The strong adsorption force is conducive to the reduction reaction. The intermediate with a weak adsorption force falls off the catalyst surface, and CH_4 cannot be obtained. The reaction path of carbene is a deoxygenation reaction, $CO_2 \rightarrow CO \rightarrow \cdot C \rightarrow \cdot CH_3 \rightarrow CH_4$. This reaction has an important intermediate product CO. If CO has a strong adsorption force on the catalyst surface, it can continue to obtain electrons for the reaction. Another important intermediate is $\cdot CH_3$ which reacts with H· to produce CH_4. For these two reaction pathways, Electron paramagnetic resonance (EPR) detection technology could be used to characterize the unpaired electron intermediates to disclose the reaction pathways.

4.3 Dry reforming methane

Dry reforming methane (DRM) by using is a method of effectively utilizing CO_2[102], CH_4 to cata-

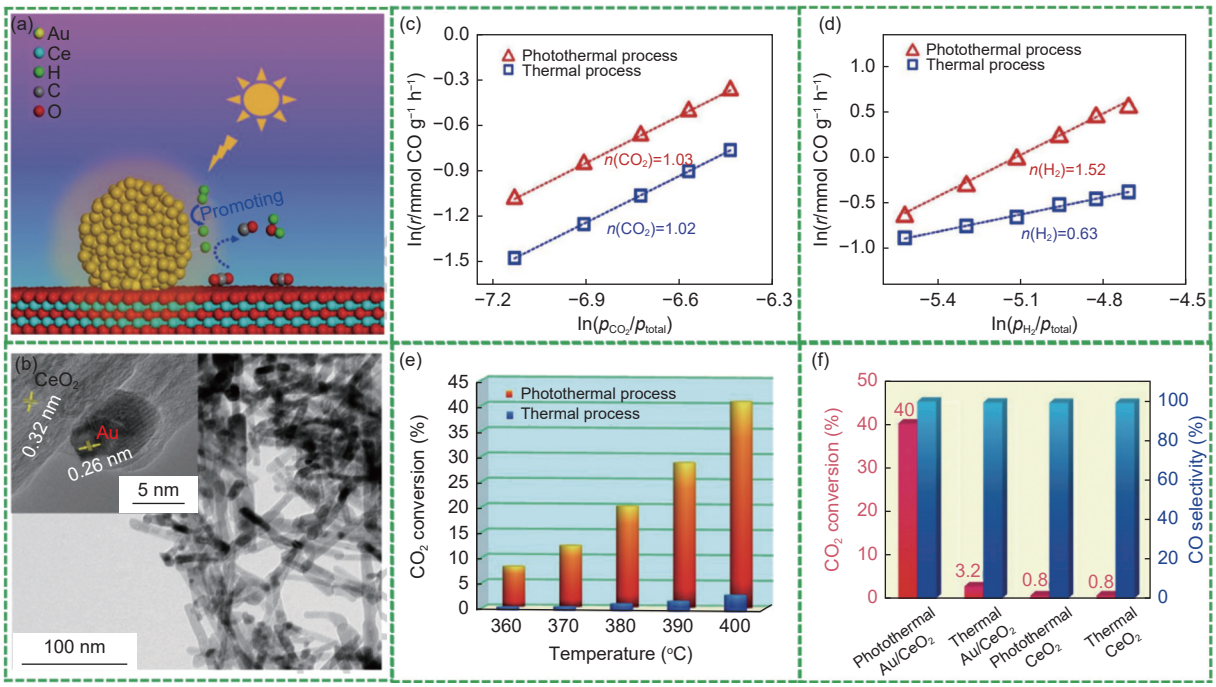

Fig. 15 (a) Schematic diagram of enhanced carbon dioxide hydrogenation in photothermal process with Au/CeO_2. (b) TEM image of Au/CeO_2 sample. The inset figure on top is the corresponding HRTEM image. Estimation of (c) CO_2 and (d) hydrogen orders from the dependence of kinetic rate on the reactant partial pressure in photothermal or thermal processes over the Au/CeO_2 catalysts at 673 K. (e) CO_2 conversion on Au/CeO_2 in the photothermal or thermal process. (f) CO_2 conversion &CO selectivity on Au/CeO_2 or CeO_2 catalysts at 400 °C under different conditions. Copyright 2019 Elsevier Inc

lyze the reduction of CO_2 and produce syngas and. Thermodynamic analysis shows that DRM is a strongly endothermic reaction, and high temperature is conducive to the forward reaction (Eq. (5))[103]. But too high reaction temperature needs higher requirements for the reaction device. And at the same time, according to Equation (4), it is prone to reverse the water gas side reaction, which consumes the generated H_2, resulting in the volume of H_2/CO decreased.

$$CO_2 + CH_4 \leftrightarrow 2CO + 2H_2 \quad \Delta H_{298K} = 247.3 \ \text{kJ} \cdot \text{mol}^{-1} \quad (5)$$

The study of the reaction mechanism is of great significance for guiding the synthesis of high-efficiency catalysts[104]. The DRM reaction mechanism is complex, and usually involves the following main steps: (i) Dissociation or activation of CH_4 and CO_2; (ii) Adsorption of intermediates on active sites; (iii) Surface reaction and product formation[105]; (iv) Desorption of products such as CO, H_2 and H_2O. Zhao et al. reported Ni_xFe_y nanoalloys synthesized from NiFeAl layered double hydroxide precursors as catalysts for DRM[106].

4.4 Other reaction

The synthesis of other hydrocarbon materials (methanol, C_{2+}) by adding H_2 to CO_2 is an exothermic reaction in terms of thermodynamics[107]. However, considering the reaction rate and the chemical inertness of CO_2, appropriately increasing the reaction temperature can make the CO_2 molecule activate and improve the reaction rate of methanol synthesis (Eq. (6))[108]. In addition, increasing the pressure of the reaction system is favorable for the reaction to proceed in the direction of producing methanol.

$$CO_2 + 3H_2 \leftrightarrow CH_3OH + H_2O \quad \Delta H_{298K} = -49.5 \ \text{kJ} \cdot \text{mol}^{-1} \quad (6)$$

It is generally supposed that CO_2 reacts with H_2 to generate CO (reverse water gas reaction), and then CO reacts with H_2 to generate methanol. Zhang et al. prepared a series of different novel iron-based catalysts by hydrogen reduction of magnesium-layered double hydroxide nanosheets at temperatures of 300–700 °C[109]. Fe-500 exhibits excellent activity for the photothermal conversion of carbon dioxide.

5 Conclusions and outlook

Photothermal catalysis plays a synergistic effect, rather than a simple superposition of photocatalysis and thermal catalysis. Photothermal catalysis is a new method to achieve high catalytic efficiency, which has a very broad prospect. The performance of photothermal catalysis is usually higher than photocatalysis or thermal catalysis, and it is a new way to realize environmental protection and comprehensive utilization of carbon resources. In this paper, we reviewed the development of photothermal catalysis from principles, and materials to applications in reduction of CO_2. The specific statements and outlook can be summarized as follows:

(1) We have discussed the difference in concept, reactors, principles, types, and applications in photothermal catalysis CO_2 reduction reaction, which is helpful to have a more comprehensive understanding of photothermal catalysis.

(2) We have draught up some photothermal catalysts materials (such as new carbon materials, oxide materials, metal sulfide materials, MOFs materials, etc.), and described their application in the CO_2 reduction. To improve the performance of the catalyst, we also have come up with some methods to modify the surface of the catalyst including heterojunction, defecting, doping, and scaling, which affect the reaction efficiency and product selectivity of the photothermal catalytic CO_2 reduction reaction.

(3) We listed some applications of photothermal catalysis CO_2 reduction, including RWGS reaction, methanation reaction, dry reforming methane, and other carbon materials synthesis.

Although photothermal catalysis has been applied in many fields, it still has some challenges.

(1) At present, most catalysts are synthesized in laboratory without consideration of cost. Once it is used in industry in the future, the cost will also be an important factor affecting whether photothermal catalysis can be popularized on a large scale. So we should look for cheap catalyst materials that are available, renewable, and environmentally friendly. Car-

bon materials may be ideal materials that are renewable and widely distributed throughout the Earth. However, a lot of them haven't been exploited yet. In the future, we should focus on new carbon materials and strive to develop cheap, efficient, recyclable, and environmentally friendly catalysts.

(2) The surface structure of the catalyst have a apparent influence on the photothermal catalytic performance, and the surface modification of the catalyst should be carried out to improve the conversion rate of CO_2. In the future, materials with specific structures would be precisely synthesized based on the relationships between structure and performance.

(3) To accurately compare the performance of different photothermal catalytic materials, parameters such as light intensity, temperature, catalyst quality, and pressure, must have a uniform evaluation criteria. Currently, this hinders comparisons between different reactions due to the lack of accurate and uniform evaluation criteria. Although some researchers have been aware of this problem, they have not yet reached a consensus. In the future, a unified testing and evaluation method should be formed to support industrialization.

After solving these challenges, photothermal catalysis is expected to have a broad application in CO_2 reduction.

Acknowledgements

This work is supported by Zhejiang Engineering Research Center of MEMS (No.MEMSZJERC2205), Postdoctoral Science Foundation, China (No. 2021M692459), and the Natural Science Foundation of Zhejiang Province, China (No. LQ21B030005).

References

[1] Li X, Yu J, Jaroniec M, et al. Cocatalysts for selective photoreduction of CO_2 into solar fuels[J]. Chemical Reviews, 2019, 119(6): 3962.

[2] Guo Q, Liang F, Li X, et al. Efficient and selective CO_2 reduction integrated with organic synthesis by solar energy[J]. Chemistry, 2019, 5(10): 2605.

[3] She X, Wang Y, Xu H, et al. Challenges and opportunities of electrocatalytic CO_2 reduction to chemicals and fuels[J]. Angewandte Chemie International Edition, 2022, 61(49): 202211396.

[4] Liang Y T, Vijayan B, Gray K, et al. Minimizing graphene defects enhances titania nanocomposite-based photocatalytic reduction of CO_2 for improved solar fuel production[J]. Nano Letters, 2011, 11(7): 2865.

[5] Lee W, Li C, Prajitno H, et al. Recent trend in thermal catalytic low temperature CO_2 methanation: A critical review[J]. Catalysis Today, 2021, 368: 2.

[6] He Y, Zhou Y, Feng J, et al. Photothermal conversion of CO_2 to fuel with nickel-based catalysts: A review[J]. Environmental Functional Materials, 2022, 1(2): 204-217.

[7] Chueh W, Falter C, Abbott M, et al. A High-flux solar-driven thermochemical dissociation of CO_2 and H_2O using nonstoichiometric ceria[J]. Science, 2010, 330(6012): 1797.

[8] Ghuman K, Wood T, Hoch L, et al. Illuminating CO_2 reduction on frustrated Lewis pair surfaces: investigating the role of surface hydroxides and oxygen vacancies on nanocrystalline $In_2O_{3-x}(OH)_y$[J]. Physical Chemistry Chemical Physics, 2015, 17(22): 14623.

[9] Zheng Y, Wu J, Zhang L, et al. Unravelling the pore templating effect on CO_2 adsorption performance of alkali metal nitrates promoted MgO pellets[J]. Chemical Engineering Journal, 2022, 450: 137944.

[10] Huang P, Guo Y, Wang G, et al. Insights into nickel-based dual function materials for CO_2 sorption and methanation: effect of reduction temperature[J]. Energy & Fuels, 2021, 35(24): 20185.

[11] Song C, Liu X, Xu M, et al. Photothermal conversion of CO_2 with tunable selectivity using Fe-based catalysts: from oxide to carbide[J]. ACS Catalysis, 2020, 10(18): 10364.

[12] Wei S, Gao J, Wu P, et al. Bi and Al co-doped anatase titania for photosensitized degradation of Rhodamine B under visible-light irradiation[J]. Ceramics International, 2021, 47(20): 28296.

[13] Zhang H, Wang T, Wang J, et al. Surface-plasmon-enhanced photodriven CO_2 reduction catalyzed by metal-organic-framework-derived iron nanoparticles encapsulated by ultrathin carbon layers[J]. Advanced Materials, 2016, 28(19): 3703.

[14] Song C, Wang Z, Yin Z, et al. Principles and applications of photothermal catalysis[J]. Chem Catalysis, 2022, 2(1): 52.

[15] O'Brien P, Sandhel A, Wood T, et al. Photomethanation of gaseous CO_2 over Ru/Silicon nanowire catalysts with visible and near-infrared photons[J]. Advanced Science, 2014, 1(1): 1400001.

[16] Li X, Wang W, Dong F, et al. Recent advances in noncontact external-field-assisted photocatalysis: from fundamentals to applications[J]. ACS Catalysis, 2021, 11(8): 4739.

[17] Wang J, Li S, Yang K, et al. Bacitracin-controlled BiO/Bi_5O_7 nanosheet assembly and S-scheme heterojunction formation for enhanced photocatalytic performances[J]. ACS Applied Nano Materials, 2022, 5(5): 6736.

[18] Nguyen H. Reticular materials for artificial photoreduction of

CO_2[J]. Advanced Energy Materials, 2020, 10(46): 2002091.

[19] Thompson W, Fernandez E, Maroto-Valer M. Review and analysis of CO_2 photoreduction kinetics[J]. ACS Sustainable Chemistry & Engineering, 2020, 8(12): 4677-4692.

[20] Xie S, Zhang Q, Liu G, et al. Photocatalytic and photoelectrocatalytic reduction of CO_2 using heterogeneous catalysts with controlled nanostructures[J]. Chemical Communications, 2016, 52(1): 35.

[21] Guo X, He H, Traitangwong A, et al. Ceria imparts superior low temperature activity to nickel catalysts for CO_2 methanation[J]. Catalysis Science & Technology, 2019, 9(20): 5636.

[22] Xie B, Wong R, Tan T, et al. Synergistic ultraviolet and visible light photo-activation enables intensified low-temperature methanol synthesis over copper/zinc oxide/alumina[J]. Nature Communications, 2020, 11(1): 1615.

[23] Wang Y, Zhang Y, Wang Y, et al. Constructing van der Waals heterogeneous photocatalysts based on atomically thin carbon nitride sheets and graphdiyne for highly efficient photocatalytic conversion of CO_2 into CO[J]. ACS Applied Materials Interfaces, 2021, 13(34): 40629.

[24] Xu F, Meng K, Zhu B, et al. Graphdiyne: A new photocatalytic CO_2 reduction cocatalyst[J]. Advanced Functional Materials, 2019, 29 (43).

[25] Cao S, Shen B, Tong T, et al. 2D/2D Heterojunction of ultrathin MXene/Bi_2WO_6 nanosheets for improved photocatalytic CO_2 reduction[J]. Advanced Functional Materials, 2018, 28 (21).

[26] Tang Q, Sun Z, Deng S, et al. Decorating g-C_3N_4 with alkalinized Ti_3C_2 MXene for promoted photocatalytic CO_2 reduction performance[J]. Journal of Colloid and Interface Science, 2020, 564: 406.

[27] Shen J, Li C, Zhang C, et al. Emerging applications of MXene materials in CO_2 photocatalysis[J]. FlatChem, 2021, 28: 100252.

[28] Low J, Zhang L, Tong T, et al. TiO_2/MXene Ti_3C_2 composite with excellent photocatalytic CO_2 reduction activity[J]. Journal of Catalysis, 2018, 361: 255.

[29] Ye M, Wang X, Liu E, et al. Boosting the photocatalytic activity of P25 for carbon dioxide reduction by using a surface-alkalinized titanium carbide MXene as cocatalyst[J]. ChemSusChem, 2018, 11(10): 1606.

[30] Li J, Wang Z, Chen H, et al. A surface-alkalinized Ti_3C_2 MXene as an efficient cocatalyst for enhanced photocatalytic CO_2 reduction over ZnO[J]. Catalysis Science & Technology, 2021, 11(14): 4953.

[31] Wu Z, Li C, Li Z, et al. Niobium and titanium carbides (MXenes) as superior photothermal supports for CO_2 photocatalysis[J]. ACS Nano, 2021, 15(3): 5696.

[32] Tahir M, Tahir B. Constructing S-scheme 2D/0D g-C_3N_4/TiO_2 NPs/MPs heterojunction with 2D-Ti_3AlC_2 MAX cocatalyst for photocatalytic CO_2 reduction to CO/CH_4 in fixed-bed and monolith photoreactors[J]. Journal of Materials Science & Technology, 2022, 106: 195.

[33] Xu M, Hu X, Wang S, et al. Photothermal effect promoting CO_2 conversion over composite photocatalyst with high graphene content[J]. Journal of Catalysis, 2019, 377: 652.

[34] Wei G, Zheng D, Xu L, et al. Photothermal catalytic activity and mechanism of $LaNixCo_{1-x}O_3$($0 \leqslant x \leqslant 1$) perovskites for CO_2 reduction to CH_4 and CH_3OH with H_2O[J]. Materials Research Express, 2019, 6 (8).

[35] Xu C, Huang W, Li Z, et al. Photothermal coupling factor achieving CO_2 reduction based on palladium-nanoparticle-loaded TiO_2[J]. ACS Catalysis, 2018, 8(7): 6582.

[36] Kho E, Jantarang S, Zheng Z, et al. Harnessing the beneficial attributes of ceria and titania in a mixed-oxide support for nickel-catalyzed photothermal CO_2 methanation[J]. Engineering, 2017, 3(3): 393.

[37] Mateo D, Morlanes N, Maity P, et al. Efficient visible - light driven photothermal conversion of CO_2 to methane by nickel nanoparticles supported on barium titanate[J]. Advanced Functional Materials, 2020, 31(8): 2008244.1-2008244.6.

[38] Wang L, Wang Y, Cheng Y, et al. Hydrogen-treated mesoporous WO_3 as a reducing agent of CO_2 to fuels (CH_4 and CH_3OH) with enhanced photothermal catalytic performance[J]. Journal of Materials Chemistry A, 2016, 4(14): 5314.

[39] Wang L, Liu X, Dang Y, et al. Enhanced solar induced photo-thermal synergistic catalytic CO_2 conversion by photothermal material decorated TiO_2[J]. Solid State Sciences, 2019, 89: 67.

[40] Jantarang S, Ligori S, Horlyck J, et al. Plasma-induced catalyst support defects for the photothermal methanation of carbon dioxide[J]. Materials (Basel), 2021, 14(15): 4195.

[41] Li D, Huang Y, Li S, et al. Thermal coupled photoconductivity as a tool to understand the photothermal catalytic reduction of CO_2[J]. Chinese Journal of Catalysis, 2020, 41(1): 154.

[42] Fiorenza R, Bellardita M, Balsamo S, et al. A solar photothermocatalytic approach for the CO_2 conversion: investigation of different synergisms on CoO-CuO/brookite TiO_2-CeO_2 catalysts[J]. Chemical Engineering Journal, 2022, 428.

[43] Tian J, Ren Y, Liu L, et al. Photothermal catalysis for CO_2 convert into C1 –C3 hydrocarbons by proton conductor BZCY532[J]. Materials Research Express, 2020, 7 (8).

[44] Ge H, Kuwahara Y, Kusu K, et al. Ru/H_xMoO_{3-y} with plasmonic effect for boosting photothermal catalytic CO_2 methanation[J]. Applied Catalysis B:Environmental, 2022, 317: 121734.

[45] Kang X, Yuan D, Yi Z, et al. Bismuth single atom supported CeO_2 nanosheets for oxidation resistant photothermal reverse water gas shift reaction[J]. Catalysis Science & Technology, 2022, 12(18): 5559-5564.

[46] Elavarasan M, Yang W, Velmurugan S, et al. Highly efficient photothermal reduction of CO_2 on Pd_2Cu dispersed TiO_2 photocatalyst and operando drift spectroscopic analysis of reactive intermediates[J]. Nanomaterials (Basel), 2022, 12 (3).

[47] Li Q, Gao Y, Zhang M, et al. Efficient infrared-light-driven photothermal CO_2 reduction over MOF-derived defective Ni/TiO_2[J]. Applied Catalysis B:Environmental, 2022, 303: 120905.

[48] Cao S, Wang Y, Zhu B, et al. Enhanced photochemical CO_2reduction in the gas phase by graphdiyne[J]. Journal of Materials Chemistry A, 2020, 8(16): 7671.

[49] Jiao X, Li X, Jin X, et al. Partially oxidized SnS_2 atomic layers achieving efficient visible-light-driven CO_2 reduction[J]. Journal of American Chemical Society, 2017, 139(49): 18044.

[50] Wang S, Guan B, Lou X. Construction of $ZnIn_2S_4$-In_2O_3 hierarchical tubular heterostructures for efficient CO_2 photoreduction[J]. Journal American Chemical Society, 2018, 140(15): 5037.

[51] Wang S, Guan B, Lu Y, et al. Formation of hierarchical In_2S_3-$CdIn_2S_4$ heterostructured nanotubes for efficient and stable visible light CO_2 reduction[J]. Journal American Chemical Society, 2017, 139(48): 17305.

[52] Sun D, Gao Y, Fu J, et al. Construction of a supported Ru complex on bifunctional MOF-253 for photocatalytic CO_2 reduction under visible light[J]. Chemical Communications (Camb), 2015, 51(13): 2645.

[53] Wang C, Xie Z, DeKrafft K, et al. Doping metal-organic frameworks for water oxidation, carbon dioxide reduction, and organic photocatalysis[J]. Journal of American Chemical Society, 2011, 133(34): 13445.

[54] Zhou A, Dou Y, Zhao C, et al. A leaf-branch TiO_2/carbon@MOF composite for selective CO_2 photoreduction[J]. Applied Catalysis B: Environmental, 2020: 264.

[55] Zhang H, Wei J, Dong J, et al. Efficient visible-light-driven carbon dioxide reduction by a single-atom implanted metal-organic framework[J]. Angewandte Chemie International Edtion, 2016, 55(46): 14310.

[56] Shi L, Wang T, Zhang H, et al. Electrostatic self-assembly of nanosized carbon nitride nanosheet onto a zirconium metal-organic framework for enhanced photocatalytic CO_2reduction[J]. Advanced Functional Materials, 2015, 25(33): 5360.

[57] Wang D, Huang R, Liu W, et al. Fe-based MOFs for photocatalytic CO_2 reduction: role of coordination unsaturated sites and dual excitation pathways[J]. ACS Catalysis, 2014, 4(12): 4254.

[58] Choi K, Kim D, Rungtaweevoranit B, et al. Plasmon-enhanced photocatalytic CO_2 conversion within metal-organic frameworks under visible light[J]. Journal of American Chemical Society, 2017, 139(1): 356.

[59] Qin J, Wang S, Wang X. Visible-light reduction CO_2 with dodecahedral zeolitic imidazolate framework ZIF-67 as an efficient co-catalyst[J]. Applied Catalysis B:Environmental, 2017, 209: 476.

[60] Chen W, Han B, Xie Y, et al. Ultrathin Co-Co LDHs nanosheets assembled vertically on MXene: 3D nanoarrays for boosted visible-light-driven CO_2 reduction[J]. Chemical Engineering Journal, 2020: 391.

[61] Han X, Lu B, Huang X, et al. Novel p- and n-type S-scheme heterojunction photocatalyst for boosted CO_2 photoreduction activity[J]. Applied Catalysis B: Environmental, 316 (2022):121587.

[62] He F, Zhuang J, Lu B, et al. Ni-based catalysts derived from Ni-Zr-Al ternary hydrotalcites show outstanding catalytic properties for low-temperature CO_2 methanation[J]. Applied Catalysis B: Environmental, 2021: 293.

[63] Ren J, Mebrahtu C, Palkovits R. Ni-based catalysts supported on Mg –Al hydrotalcites with different morphologies for CO_2 methanation: exploring the effect of metal–support interaction[J]. Catalysis Science & Technology, 2020, 10(6): 1902.

[64] Zhang X, Yang Y, Xiong L, et al. 3D dahlia-like NiAl-LDH/CdS heterosystem coordinating with 2D/2D interface for efficient and selective conversion of CO_2[J]. Chinese Chemical Letters, 2022, 33(4): 2111.

[65] Zheng Y, Lin L, Ye X, et al. Helical graphitic carbon nitrides with photocatalytic and optical activities[J]. Angewandte Chemie International Edtion, 2014, 53(44): 11926.

[66] Bai S, Wang X, Hu C, et al. Two-dimensional g-C_3N_4: an ideal platform for examining facet selectivity of metal co-catalysts in photocatalysis[J]. Chemical Communication (Camb), 2014, 50(46): 6094.

[67] Ma B, Chen G, Fave C, et al. Efficient visible-light-driven CO_2 reduction by a cobalt molecular catalyst covalently linked to mesoporous carbon nitride[J]. Journal of Amerian Chemical Society, 2020, 142(13): 6188.

[68] Neatu S, Macia-Agullo J, Concepcion P, et al. Gold-copper nanoalloys supported on TiO_2 as photocatalysts for CO_2 reduction by water[J]. Journal of Amerian Chemical Society, 2014, 136(45): 15969.

[69] Shan J, Raziq F, Humayun M, et al. Improved charge separation and surface activation via boron-doped layered polyhedron $SrTiO_3$ for co-catalyst free photocatalytic CO_2 conversion[J]. Applied Catalysis B:Environmental, 2017, 219: 10.

[70] Zhang Y, Du W, Wang M, et al. Synergy of yolk-shelled structure and tunable oxygen defect over CdS/ $CdCO_3$-CoS_2: Wide band-gap semiconductors assist in efficient visible-light-driven H_2 production and CO_2 reduction[J]. Chemical Engineering Journal, 2023, 454:140113

[71] Li X, Wang L, Su W, et al. A review of the research status of CO_2 photocatalytic conversion technology based on bibliometrics[J]. New Journal of Chemistry, 2021, 45(5): 2315.

[72] Xu H, Hu J, Wang D, et al. Visible-light photoreduction of CO_2 in a metal-organic framework: boosting electron-hole separation via electron trap states[J]. Journal of Amerial Chemical Society, 2015, 137(42): 13440.

[73] Chen X, Guo R, Hong L, et al. Research progress on CO_2 photocatalytic reduction with full solar spectral responses[J]. Energy & Fuels, 2021, 35(24): 19920.

[74] Tan L, Xu S, Wang Z, et al. Highly selective photoreduction of CO_2 with suppressing H_2 evolution over monolayer layered double hydroxide under irradiation above 600 nm[J]. Angewandte Chemie International Edition, 2019, 58(34): 11860.

[75] Chen G, Gao R, Zhao Y, et al. Alumina-supported CoFe alloy

catalysts derived from layered-double-hydroxide nanosheets for efficient photothermal CO_2 hydrogenation to hydrocarbons[J]. Advanced Materials, 2018, 30 (3).

[76] Vasileff A, Xu C, Jiao Y, et al. Surface and interface engineering in copper-based bimetallic materials for selective CO_2 electroreduction[J]. Chem, 2018, 4(8): 1809.

[77] Xu C, Zhang Y, Pan F, et al. Guiding effective nanostructure design for photo-thermochemical CO_2 conversion: From DFT calculations to experimental verifications[J]. Nano Energy, 2017, 41: 308.

[78] Yu J, Wang S, Low J, et al. Enhanced photocatalytic performance of direct Z-scheme g-C_3N_4-TiO_2 photocatalysts for the decomposition of formaldehyde in air[J]. Physical Chemistry Chemical Physics, 2013, 15(39): 16883.

[79] Hasija V, Kumar A, Sudhaik A, et al. Step-scheme heterojunction photocatalysts for solar energy, water splitting, CO_2 conversion, and bacterial inactivation: a review[J]. Environmental Chemistry Letters, 2021, 19(4): 2941.

[80] Xu Q, Zhang L, Cheng B, et al. S-scheme heterojunction photocatalyst[J]. Chem, 2020, 6(7): 1543.

[81] Xu F, Meng K, Cheng B, et al. Unique S-scheme heterojunctions in self-assembled TiO_2/$CsPbBr_3$ hybrids for CO_2 photoreduction[J]. Nature Communications, 2020, 11(1): 4613.

[82] Yan J, Wang C, Ma H, et al. Photothermal synergic enhancement of direct Z-scheme behavior of Bi_4TaO_8Cl/$W_{18}O_{49}$ heterostructure for CO_2 reduction[J]. Applied Catalysis B: Environmental, 2020: 268.

[83] Cai S, Chen J, Li Q, et al. Enhanced photocatalytic CO_2 reduction with photothermal effect by cooperative effect of oxygen vacancy and Au cocatalyst[J]. ACS Applied Materials Interfaces, 2021, 13(12): 14221.

[84] Zhang M, Lu M, Lang Z, et al. Semiconductor/covalent-organic-framework Z-scheme heterojunctions for artificial photosynthesis[J]. Angewandte Chemie International Edition, 2020, 59(16): 6500.

[85] Li J, Ye Y, Ye L, et al. Sunlight induced photo-thermal synergistic catalytic CO_2 conversion via localized surface plasmon resonance of MoO_{3-x}[J]. Journal of Materials Chemistry A, 2019, 7(6): 2821.

[86] Yu F, Wang C, Li Y, et al. Enhanced solar photothermal catalysis over solution plasma activated TiO_2[J]. Advanced Science, 2020, 7 (16): 2000204.

[87] Li Z, Zhang X, Zhang L, et al. Pathway alteration of water splitting via oxygen vacancy formation on anatase titanium dioxide in photothermal catalysis[J]. The Journal of Physical Chemistry C, 2020, 124(48): 26214.

[88] Duan C, Ding M, Feng Y, et al. ZIF-L-derived ZnO/N-doped carbon with multiple active sites for efficient catalytic CO_2 cycloaddition[J]. Separation and Purification Technology, 2022, 285: 120359.

[89] Qi Y, Jiang J, Liang X, et al. Fabrication of black In_2O_3 with dense oxygen vacancy through dual functional carbon doping for enhancing photothermal CO_2 hydrogenation[J]. Advanced Functional Materials, 2021, 31 (22).

[90] Li Z, Zhang L, Huang W, et al. Photothermal catalysis for selective CO_2 reduction on the modified anatase TiO_2 (101) surface[J]. ACS Applied Energy Materials, 2021, 4(8): 7702.

[91] Zhao T, Yang Z, Tang Y, et al. Advances and perspectives of photopromoted CO_2 hydrogenation for methane production: catalyst development and mechanism investigations[J]. Energy & Fuels, 2022, 36(13): 6711.

[92] Wang L, Chen W, Zhang D, et al. Surface strategies for catalytic CO_2 reduction: from two-dimensional materials to nanoclusters to single atoms[J]. Chemical Society Reviews, 2019, 48(21): 5310.

[93] Liu L, Corma A. Metal catalysts for heterogeneous catalysis: from single atoms to nanoclusters and nanoparticles[J]. Chemical Reviews, 2018, 118(10): 4981.

[94] Yang Q, Yang C, Lin C, et al. Metal-organic-framework-derived hollow N-doped porous carbon with ultrahigh concentrations of single Zn atoms for efficient carbon dioxide conversion[J]. Angewandte Chemie International Edition, 2019, 58(11): 3511.

[95] Lee S, Jeong S, Kim W, et al. Low-coordinated surface atoms of CuPt alloy cocatalysts on TiO_2 for enhanced photocatalytic conversion of CO_2[J]. Nanoscale, 2016, 8(19): 10043.

[96] Bahmanpour A, Signorile M, Kröcher. Recent progress in syngas production via catalytic CO_2 hydrogenation reaction[J]. Applied Catalysis B: Environmental, 2021: 295.

[97] Wang Z, Song H, Liu H, et al. Coupling of solar energy and thermal energy for carbon dioxide reduction: status and prospects[J]. Angewandte Chemie International Edition, 2020, 59(21): 8016.

[98] Su X, Yang X, Zhao B, et al. Designing of highly selective and high-temperature endurable RWGS heterogeneous catalysts: recent advances and the future directions[J]. Journal of Energy Chemistry, 2017, 26(5): 854.

[99] Lu B, Quan F, Sun Z, et al. Photothermal reverse-water-gas-shift over Au/CeO_2 with high yield and selectivity in CO_2 conversion[J]. Catalysis Communications, 2019: 129.

[100] Fu J, Jiang K, Qiu X, et al. Product selectivity of photocatalytic CO_2 reduction reactions[J]. Materials Today, 2020, 32: 222.

[101] Habisreutinger S, Schmidt-Mende L, Stolarczyk J. Photocatalytic reduction of CO_2 on TiO_2 and other semiconductors[J]. Angewandte Chemie International Edition, 2013, 52(29): 7372.

[102] Zhao Y, Waterhouse G, Chen G, et al. Two-dimensional-related catalytic materials for solar-driven conversion of CO_x into valuable chemical feedstocks[J]. Chemical Society Reviews, 2019, 48(7): 1972.

[103] Wittich K, Krämer M, Bottke N, et al. Catalytic dry reforming of methane: insights from model systems[J]. ChemCatChem, 2020, 12(8): 2130.

[104] Kathiraser Y, Oemar U, Saw E, et al. Kinetic and mechanistic aspects for CO_2 reforming of methane over Ni based catalysts[J]. Chemical Engineering Journal, 2015, 278: 62.

[105] Foppa L, Silaghi M, Larmier K, et al. Intrinsic reactivity of Ni, Pd

and Pt surfaces in dry reforming and competitive reactions: Insights from first principles calculations and microkinetic modeling simulations[J]. Journal of Catalysis, 2016, 343: 196.

[106] Zhao J, Guo X, Shi R, et al. NiFe nanoalloys derived from layered double hydroxides for photothermal synergistic reforming of CH_4 with CO_2[J]. Advanced Functional Materials, 2022: 2204056.

[107] Chen G, Waterhouse G, Shi R, et al. From solar energy to fuels: recent advances in light-driven C1 chemistry[J]. Angewandte Chemie International Edition, 2019, 58(49): 17528.

[108] Sharma P, Sebastian J, Ghosh S, et al. Recent advances in hydrogenation of CO_2 into hydrocarbons via methanol intermediate over heterogeneous catalysts[J]. Catalysis Science & Technology, 2021, 11(5): 1665.

[109] Li Z, Liu J, Shi R, et al. Fe - based catalysts for the direct photohydrogenation of CO_2 to value - added hydrocarbons[J]. Advanced Energy Materials, 2021, 11(12).

光热催化在二氧化碳还原反应中的原理，材料和应用

赵善海[1,†]， 王海兵[1,†]， 李 强[2]， 丁 皓[1]， 钱 程[1]， 汪 琪[2]，
李慧玉[1]， 蒋 锋[1]， 曹海静[1,*]， 李春鹤[2,*]， 朱燕艳[1,*]

（1. 上海电力大学 数理学院，上海 200090；
2. 绍兴文理学院 数理信息学院，浙江 绍兴 312000）

摘 要： 碳元素消耗导致了大量的 CO_2 排放，这引起了人们的广泛关注。发展可再生能源和减少 CO_2 排放的技术已成为世界上最迫切需要解决的问题之一。其中，太阳能作为地球上最理想的清洁能源，已成为当前研究的热点。如果可以利用太阳能将 CO_2 转化为有价值的碳基化学品，以上两个问题可以同时解决。光催化法和热催化法在 CO_2 还原中的应用已有许多报道。但关于光热催化还原二氧化碳的研究较少。本文综述了光热催化在 CO_2 还原中的研究现状，介绍了光热催化的概念和原理，催化剂的分类（新型炭材料、氧化物材料、金属硫化物材料、MOF 材料、层状双氢氧化物材料）和催化剂的改性，以及其在 CO_2 还原方面的应用。最后，本文对催化剂的发展趋势进行了预测。因此，合理开发碳基化学品可以减少传统能源的消耗、碳排放，实现碳的循环利用。

关键词： 光热催化；二氧化碳还原反应；TiO_2；MOF；异质结

中图分类号： $TQ127.1^{+}1$ **文献标识码：** A

基金项目： 微机电系统浙江省工程研究中心 (No.MEMSZJERC2205)；中国博士后科学基金 (No. 2021M692459)；浙江省自然科学基金 (No. LQ21B030005).

通讯作者： 曹海静，副教授. E-mail: caohj@shiep.edu.cn；
李春鹤，副教授. E-mail: chunhe@whu.edu.cn；
朱燕艳，教授. E-mail: yyzhu@shiep.edu.cn

作者简介： †赵善海和王海兵为共同第一作者

本文的电子版全文由 Elsevier 出版社在 ScienceDirect 上出版（https://www.sciencedirect.com/journal/new-carbon-materials/）